ETHzürich

Heteronuclear filters in two-dimensional [1H, 1H]-NMR spectroscopy: combined use with isotope labelling for studies of macromolecular conformation and intermolecular interactions

Heteronuclear filters in two-dimensional [¹H,¹H]-NMR spectroscopy: combined use with isotope labelling for studies of macromolecular conformation and intermolecular interactions

GOTTFRIED OTTING AND KURT WÜTHRICH

*Institut für Molekularbiologie und Biophysik, Eidgenössische Technische Hochschule–Hönggerberg,
CH-8093 Zürich, Switzerland*

I. INTRODUCTION

The use of heteronuclear filters enables the editing of complex ¹H nuclear magnetic resonance (NMR) spectra into simplified subspectra containing a lesser number of resonance lines, which are then more easily amenable to detailed spectral analysis. This editing is based on the creation of heteronuclear two-spin or multiple-spin coherence and discrimination between protons that do or do not participate in these heteronuclear coherences. In principle, heteronuclear editing can be used in conjunction with one-dimensional or multidimensional ¹H-NMR experiments for studies of a wide variety of low-molecular-weight compounds or macromolecular systems, and is implicitly applied in a wide range of heteronuclear NMR experiments with proton detection (e.g. Bax *et al.* 1983; Griffey & Redfield, 1987). In the present article we shall focus on the use of heteronuclear filters in two-dimensional (2D) [¹H,¹H]-NMR experiments. The selection of the material covered was primarily motivated by its impact on the practice of protein structure determination in solution, and on NMR studies of intermolecular interactions with biological macromolecules. Section 2 surveys potential applications of heteronuclear filters in this area. The remainder of the article is devoted to an introduction of the theoretical principles used in heteronuclear filters, and to a detailed description of the experimental implementation of these measurements. In writing the review we tried to minimize redundancy with the recent article in *Quarterly Review of Biophysics* by Griffey & Redfield (1987) and to concentrate on experiments that were introduced during the period 1986–9.

The practical significance of the experimental procedures discussed in this review is best assessed within the general framework of the NMR method for structure determination of biological macromolecules in solution (Wüthrich, 1986, 1989). Generally, heteronuclear filters can help in important ways to extend the use of this methodology to more complex systems, including bigger molecules and multimolecular aggregates. Similar to heteronuclear three-dimensional (3D)

Table 1. *Survey of the editing characteristics of heteronuclear filters in homonuclear 2D [¹H,¹H]-NMR experiments*

Filter	Selected coherence[a]	Tuning[b]	Subspectrum	Protons observed[c] ω₁	Protons observed[c] ω₂
X-filter	HX	No	Difference	H(X)	H'(X)
			Sum	I and H	I' and H'
2X-filter	HXX'	No	Difference	H(X and X')	H'(X and X')
			Sum	I and H	I' and H'
X(ω₁)-half-filter[d]	HX	Yes (τ)	Difference	H(X)	I and H'
			Sum	I[e]	I' and H
X(ω₂)-half-filter[d]	HX	Yes (τ)	Difference	I and H	H(X)
			Sum	I and H	I'[e]
X(ω₁ω₂)-double-half-filter[d]	HX(τ₁), HX(τ²)	Yes (τ₁,τ₂)	X(ω₁)-X(ω₂)-doubly-selected	H(X)	H'(X or X')
			X(ω₁)-filtered/X(ω₂)-selected	I'	H(X)
			X(ω₁)-selected/X(ω₂)-filtered	H(X)	I'
			X(ω₁)-X(ω₂)-doubly-filtered	I'	I'[f]

[a] The types of participating spins are identified and their number indicates the order of coherence. X and X' are heteronuclear spins of the same isotope. H designates protons that interact with X in a way that is recognized by the filter used: with nX-filters, these are all the protons with nonvanishing couplings $\mathcal{J}_{HX}$ to n different X-spins. With X-half-filters and X-double-half-filters these are usually only those protons which are directly bonded to X and have large one-bond coupling constants.

[b] τ, τ_1 and τ_2 are tuning delays in the half-filter elements.

[c] The information in parentheses indicates the number of heteronuclear spins to which the observable protons must be coupled, and specifies whether the protons observable in ω_1 and in ω_2 must be coupled to the same hetero spins. I designates all the protons that are not classified as H and are not recognized by the filter [see footnote (a)]. H and H', or I and I', respectively, are identical spins for the diagonal peaks and different spins for the cross-peaks.

[d] In an analogous fashion to the X-half-filters, 2X-half-filters and higher order half-filters can be devised. All these half-filter elements can also be combined in experiments with heteronuclear double-half-filters.

[e] For an optimally tuned filter delay, with $\tau = 1/2\mathcal{J}_{HX}$.

[f] For optimally tuned filter delays, with $\tau_1 = 1/2\mathcal{J}_{HX}$ and $\tau_2 = 1/2\mathcal{J}'_{HX}$, where $\mathcal{J}_{HX}$ and $\mathcal{J}'_{HX}$ may have identical or different values.

NMR, which is also reviewed in this issue of *Quarterly Reviews of Biophysics* (Fesik & Zuiderweg, 1990), the potentialities of heteronuclear filters can be greatly enhanced by combination with suitable isotope labelling techniques. This includes, for example, biosynthetically directed fractional labelling (Senn *et al.* 1989; Neri *et al.* 1989) or selective labelling by residue-type, which both can efficiently be obtained for recombinant proteins. Relative to heteronuclear 3D NMR the use of 2D [^{1}H,^{1}H]-NMR with heteronuclear filters may for certain applications be a valid alternative, both for fundamental as well as for practical reasons, and there are other applications where heteronuclear filters will foreseeably be the most powerful approach, especially for studies of intermolecular interactions with biological macromolecules (Fesik *et al.* 1988; Senn *et al.* 1987*b*).

2. APPLICATIONS OF HETERONUCLEAR FILTERS IN ^{1}H-NMR STUDIES OF BIOLOGICAL MACROMOLECULES

Table 1 gives a survey of the heteronuclear filters that are discussed in this review. The names listed in the first column indicate the *order* of the filter and distinguish between *filters* and *half-filters*. The order n of a nX-filter or a nX-half-filter indicates the number of heteronuclear spins, X, to which a proton must be coupled in order to be recognized by the filter. For example, X-filters select for protons with a non-vanishing coupling constant J_{HX} to a single heteronuclear spin, 2X-filters for those with two non-vanishing coupling constants to two heteronuclear spins X and X'. Higher order filters can be devised, but they are hardly of practical interest.

The practical significance of heteronuclear filtering can best be appreciated on the background of some facts on conventional 2D [^{1}H,^{1}H]-NMR spectra (Ernst *et al.* 1987; Wüthrich, 1986). The 2D [^{1}H,^{1}H]-NMR spectra of prime importance for work with biological macromolecules contain an array of diagonal peaks in the 2D frequency plane (Fig. 1*b*), with $\omega_1 = \omega_2$, which display the chemical shift positions of the resonance lines and resemble the conventional 1D spectrum (Fig. 1*a*). In addition, there are a large number of cross-peaks with $\omega_1 \neq \omega_2$. These come about by correlation of individual resonance lines in the 1D ^{1}H-NMR spectrum along ω_2 (Fig. 1*a*) with different individual lines in the same ^{1}H-NMR spectrum displayed along ω_1 (not shown in Fig. 1). Depending on the experiment used, the cross-peaks manifest different types of interactions between proton spins, and thus contain the desired information needed for the determination of the molecular structure (Wüthrich, 1986, 1989). For example, in 2D nuclear Overhauser enhancement spectroscopy (NOESY) the cross-peaks represent nuclear Overhauser effects (NOE), which indicate that the protons corresponding to the two correlated peaks are separated only by a short distance, say less than 5·0 Å, and in 2D correlated spectroscopy (COSY) the cross-peaks represent scalar spin–spin couplings, which indicate that the protons corresponding to the two correlated peaks are part of the same chemical structure and are separated usually by not more than three chemical bonds. Since biological macromolecules contain a large number of hydrogen atoms and a correspondingly large number of ^{1}H-
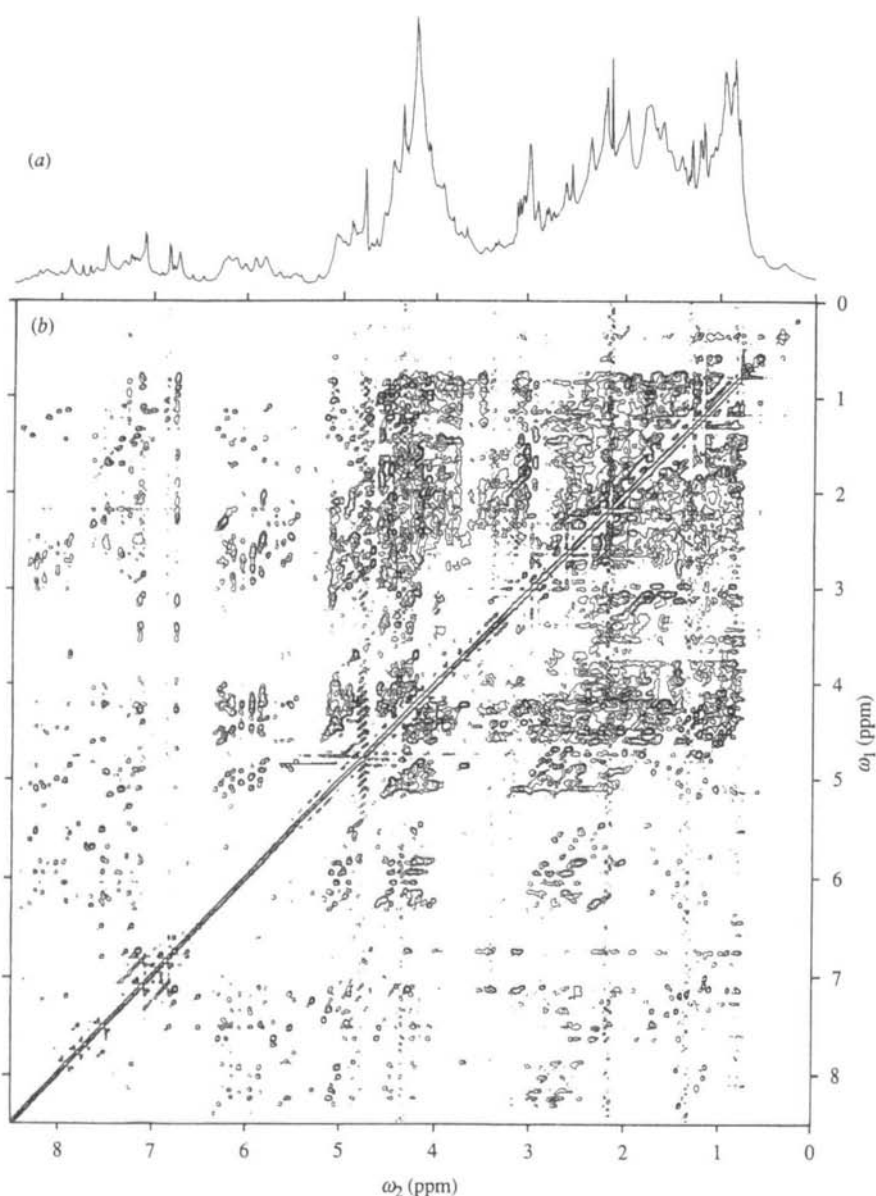
Fig. 1. ^{1}H-NMR spectra of the 1:1 complex formed between the DNA-binding domain consisting of the 76 N-terminal residues of *Salmonella* phage P22 c2 repressor and a 16 base-pair operator DNA-duplex (D$_2$O solution, complex concentration 1·5 mM, 25 mM phosphate buffer, 100 mM-KCl, pD = 6·0, T = 28 °C, proton frequency 500 MHz). (*a*) Conventional 1D spectrum. (*b*) Conventional homonuclear [^{1}H,^{1}H]-NOESY spectrum recorded with a mixing time of 100 ms.

NMR lines (Fig. 1*a*), and since there are numerous NOEs and scalar proton–proton interactions, both the diagonal and large parts of the ω_1–ω_2 plane in 2D [^{1}H,^{1}H]-NMR spectra of proteins and nucleic acids are crowded with signals (Fig. 1*b*). With increasing size of molecules studied, the resulting mutual

overlap of resonance lines becomes one of the limiting factors governing the feasibility of a detailed NMR investigation. With the insertion of a heteronuclear filter a much simpler subspectrum can be obtained because the resonances of only part of the protons in the system studied will be observable, for example, only those with non-vanishing scalar couplings to a ^{15}N nucleus.

In the practice of heteronuclear filtering pairs of 2D [^{1}H,^{1}H]-NMR spectra are recorded in an identical way except for the phase of a $(\pi/2)(X)$-editing pulse. The desired subspectra are then obtained as linear combinations of these recordings. In experiments with nX-filters or nX-half-filters two data sets are combined into two subspectra. With nX-double-half-filters, where two independent heteronuclear nX-half-filters are applied in the two frequency dimensions, four data sets are combined into four different subspectra. Depending on the combination used, the actual function of the filter may be either to select the resonances of X-coupled protons for observation in the subspectrum, or to filter X-coupled protons out of the subspectrum. The columns 4, 5 and 6 of Table 1 list the information contained in the different subspectra obtained with these procedures. The concept of using the same data sets for obtaining the different subspectra ensures that no desirable proton magnetization needs to be discarded in the course of the experiment. Each individual subspectrum has a signal-to-noise ratio which approximates that of the conventional, unfiltered spectrum. Furthermore, since all subspectra are obtained from a single experimental setup, the resonance positions of corresponding signals in the different subspectra are identical.

There are important differences between nX-filters and nX-half-filters. While a X-filter selects for X-coupled protons along both ω_1 and ω_2, a X-half-filter selects only in one frequency dimension, ω_1 *or* ω_2, and all protons are observed in the other direction. The selection along the two frequency axes by a X-filter is for pairs of protons with *non-vanishing* spin–spin couplings to the *same* heteronuclear spin. As a result, the X-filter will suppress all diagonal peaks with the exception of those corresponding to X-coupled protons, and all cross-peaks except those between pairs of protons which are both coupled to the same X spin. Table 2 affords a survey of the combinations of non-vanishing heteronuclear spin–spin couplings that are recognized by the X-filter and the 2X-filter. In contrast, with a X-half-filter a subspectrum may be obtained that contains only diagonal peaks from X-coupled protons, and cross-peaks correlating the X-coupled protons with *all* protons that interact with them, independent of whether or not these are also coupled to X ('interaction' stands here, for example, for proton–proton NOE in the case of NOESY, or for proton–proton scalar coupling in the case of COSY).

Another crucial difference between heteronuclear filters and half-filters is that nX-filters select for the *presence* of heteronuclear couplings $\mathscr{J}_{HX}$ and the filter effect is independent of the size of the coupling constants, whereas the nX-half-filters are tuned for distinct values of $\mathscr{J}_{HX}$ (column 3 of Table 1). Table 3 lists the trigonometric functions which govern the distribution of the signal intensities between the different subspectra obtained with X-half-filter elements.

The following sections 2·1 and 2·2 outline the scope of potential practical

Table 2. *Combinations of heteronuclear spin–spin couplings required for observation of diagonal peaks and cross-peaks in 2D [¹H,¹H]-NMR experiments with nX-filters*

Filter	Subspectrum[a]	Combinations of heteronuclear coupling constants required for proton observation	
		Diagonal peaks	Cross-peaks
X-Filter	Difference	$J(^1\mathrm{H},\mathrm{X}) \neq o$	$J(^1\mathrm{H},\mathrm{X}) \neq o$ and $J(^1\mathrm{H}',\mathrm{X}) \neq o$
2X-filter	Difference	$J(^1\mathrm{H},\mathrm{X}) \neq o$ and $J(^1\mathrm{H},\mathrm{X}') \neq o$ [b]	$J(^1\mathrm{H},\mathrm{X}) \neq o$ and $J(^1\mathrm{H},\mathrm{X}') \neq o$ and $J(^1\mathrm{H}',\mathrm{X}) \neq o$ and $J(^1\mathrm{H}',\mathrm{X}') \neq o$ [b]

[a] Only the difference spectra are listed. The sum spectra contain all the diagonal peaks and cross-peaks seen in the corresponding conventional 2D [¹H,¹H]-NMR experiment, and effects of the nX-filters are only manifested by alterations of the fine structure of the signals from X-coupled protons.

[b] X and X′ must be two different spins of the isotope X.

Table 3. *Trigonometric functions governing the distribution of the signal intensity of X-coupled protons between the different subspectra obtained in 2D [¹H,¹H]-NMR experiments with X-half-filter elements*

Filter	Subspectrum	Relative signal intensity[a]	
		Diagonal peaks	Cross-peaks
X(ω_1)-half-filter	Difference	$\sin(\pi J_{HX}\tau) \times 1$	$\sin(\pi J_{HX}\tau) \times 1$
	Sum	$\cos(\pi J_{HX}\tau) \times 1$	$\cos(\pi J_{HX}\tau) \times 1$
X(ω_2)-half-filter	Difference	$1 \times \sin(\pi J_{HX}\tau)$	$1 \times \sin(\pi J_{HX}\tau)$
	Sum	$1 \times \cos(\pi J_{HX}\tau)$	$1 \times \cos(\pi J_{HX}\tau)$
X(ω_1,ω_2)-double-half-filter	X(ω_1)-X(ω_2)-doubly-selected	$\sin(\pi J_{HX}\tau_1)\sin(\pi J_{HX}\tau_2)$	$\sin(\pi J_{HX}\tau_1)\sin(\pi J_{H'X'}\tau_2)$[b]
	X(ω_1)-filtered/X(ω_2)-selected	$\cos(\pi J_{HX}\tau_1)\sin(\pi J_{HX}\tau_2)$	$\cos(\pi J_{HX}\tau_1)\sin(\pi J_{H'X'}\tau_2)$[b]
	X(ω_1)-selected/X(ω_2)-filtered	$\sin(\pi J_{HX}\tau_1)\cos(\pi J_{HX}\tau_2)$	$\sin(\pi J_{HX}\tau_1)\cos(\pi J_{H'X'}\tau_2)$[b]
	X(ω_1)-X(ω_2)-doubly-filtered	$\cos(\pi J_{HX}\tau_1)\cos(\pi J_{HX}\tau_2)$	$\cos(\pi J_{HX}\tau_1)\cos(\pi J_{H'X'}\tau_2)$[b]

[a] J_{HX} designates heteronuclear spin–spin coupling constants. τ, τ_1 and τ_2 are the filter delays in the X half-filter elements (Fig. 14). The filter delay is optimally tuned with $\tau = 1/2J_{HX}$. The first term and the second term in the expressions for the signal intensities account for the filter effects along ω_1 and ω_2, respectively.

[b] X and X' may be either the same or two different spins. J_{HX} and $J_{H'X'}$ may have identical or different values.

applications for nX-filters and nX-half-filters. As we shall see, the selection of the filter type will in each instance largely depend on considerations of the filter characteristics listed in Tables 1–3.

2.1 nX-filters

X-filters, and even more pronouncedly higher order X-filters with $n = 2, 3, \ldots$, impose very stringent restrictions on the peaks selected in the 2D [^{1}H,^{1}H]-NMR difference spectra (Table 2). As a result, 2D [^{1}H,^{1}H]-NMR spectra recorded with a X-filter usually contain only a very small number of cross peaks and are therefore well resolved. Since the selection criterion is 'hard' in that there is no tunable range of spin–spin coupling constants to be chosen (Table 1), X-filters are ideally suitable for work with systems where a large spread of the values of the heteronuclear coupling constants would prevent proper tuning of a filter delay. Quite generally this situation arises in the presence of dihedral angle-dependent vicinal (i.e. between nuclear spins separated by three covalent bonds) or longer-range spin–spin coupling constants (Karplus, 1959). An illustrative example is presented by metallothionein (Fig. 2).

Mammalian metallothioneins consist of a polypeptide chain with 61 or 62 residues, which binds 7 bivalent metal ions, for example, Cd^{2+}. The 3D structure (Fig. 2) consists of two domains containing three and four metal ions, respectively. The cadmium ions are coordinated to the sulphur atoms of 20 cysteinyl side chains contained in the metallothionein amino-acid sequence (Fig. 3). Rabbit metallothionein-2a was the first protein for which isotope labelling and heteronuclear NMR experiments were used to complement ^{1}H-NMR measurements in the determination of the 3D-structure (Neuhaus *et al.* 1984; Frey *et al.* 1985; Arseniev *et al.* 1988). In the initial studies the ^{1}H-NMR lines of the metal-bound Cys were identified by a comparison of two protein preparations containing, respectively, the NMR-inactive isotope ^{112}Cd (I = 0), and the NMR-observable isotope ^{113}Cd ($I = \frac{1}{2}$) (Neuhaus *et al.* 1984). With the use of a X-filter and a 2X-filter (X = ^{113}Cd) the ^{1}H-NMR lines of Cys bound to one or two ^{113}Cd^{2+} ions could be identified directly in [^{113}Cd$_7$]-metallothionein, without the need for preparation of the [^{112}Cd$_7$]-protein.

The values of the coupling constants $^3\mathcal{J}(H^\beta, ^{113}Cd)$ and $^4\mathcal{J}(H^\alpha, ^{113}Cd)$ are dependent on the dihedral angles χ^2, or χ^1 and χ^2, respectively (Fig. 3). In rat metallothionein-2, values of the ^{1}H–^{113}Cd coupling constants were found to range from 0 to 76 Hz. Fig. 4 shows a comparison of a conventional [^{1}H,^{1}H]-COSY spectrum of rat metallothionein with the difference spectrum obtained from [^{1}H,^{1}H]-COSY with ^{113}Cd-filter. The spectral region shown contains the diagonal peaks of the C$^\alpha$-protons and the cross-peaks between the C$^\alpha$-protons (along ω_2) and the C$^\beta$-protons (along ω_1). The difference spectrum (Fig. 4b) contains only diagonal peaks from protons coupled to ^{113}Cd, and cross peaks between pairs of protons which are both coupled to the same ^{113}Cd ion. It is seen that both the diagonal resonances of C$^\alpha$-protons and cross peaks with C$^\alpha$-protons can routinely be observed, although they are related to the ^{113}Cd spins only by small four-bond

(a)

(b)
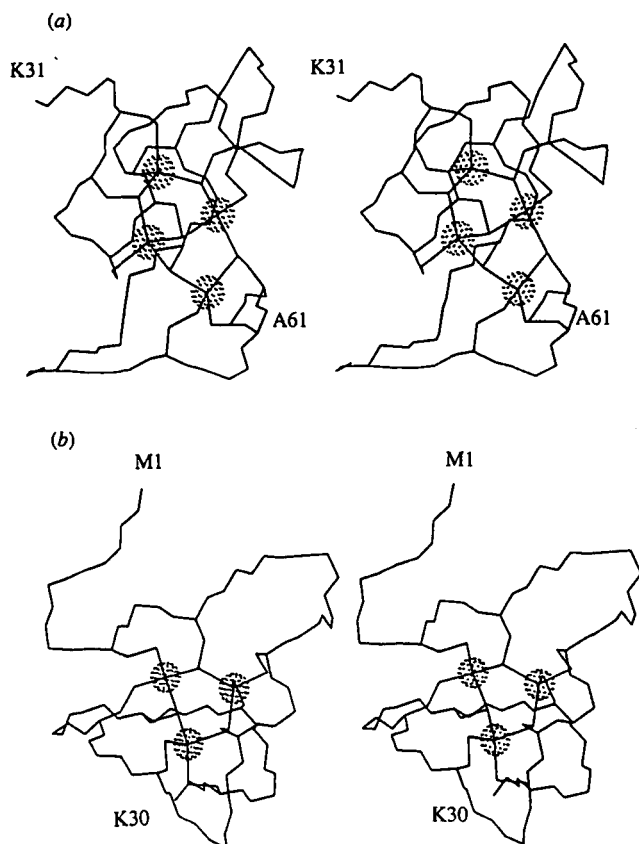
Fig. 2. Stereoview of the solution of rat metallothionein-2 determined by NMR. The positions of the polypeptide backbone atoms N, C^α and C′, and the side-chain heavy atoms of the 20 cysteinyl residues are connected by straight lines, and the cadmium ions are represented as dotted spheres of radius 0·9 Å. (a) α-domain, (b) β-domain. The first and last residues of each domain are identified by the one-letter amino-acid code and the sequence number (from Schultze *et al.* 1988).
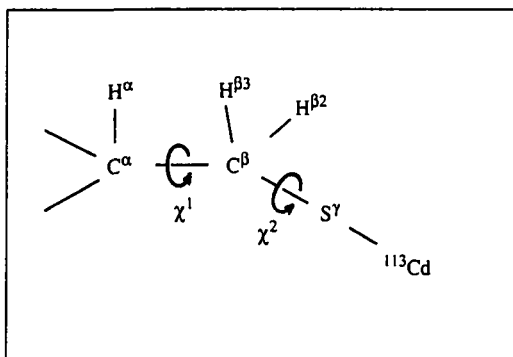
Fig. 3. Cysteine sulphur-to-^{113}Cd coordinative bond. χ^1 and χ^2 are the two dihedral angles that define the conformation of the side chain. In metallothionein 8 of the 20 cysteinyl residues are bound to two Cd^{2+} ions.
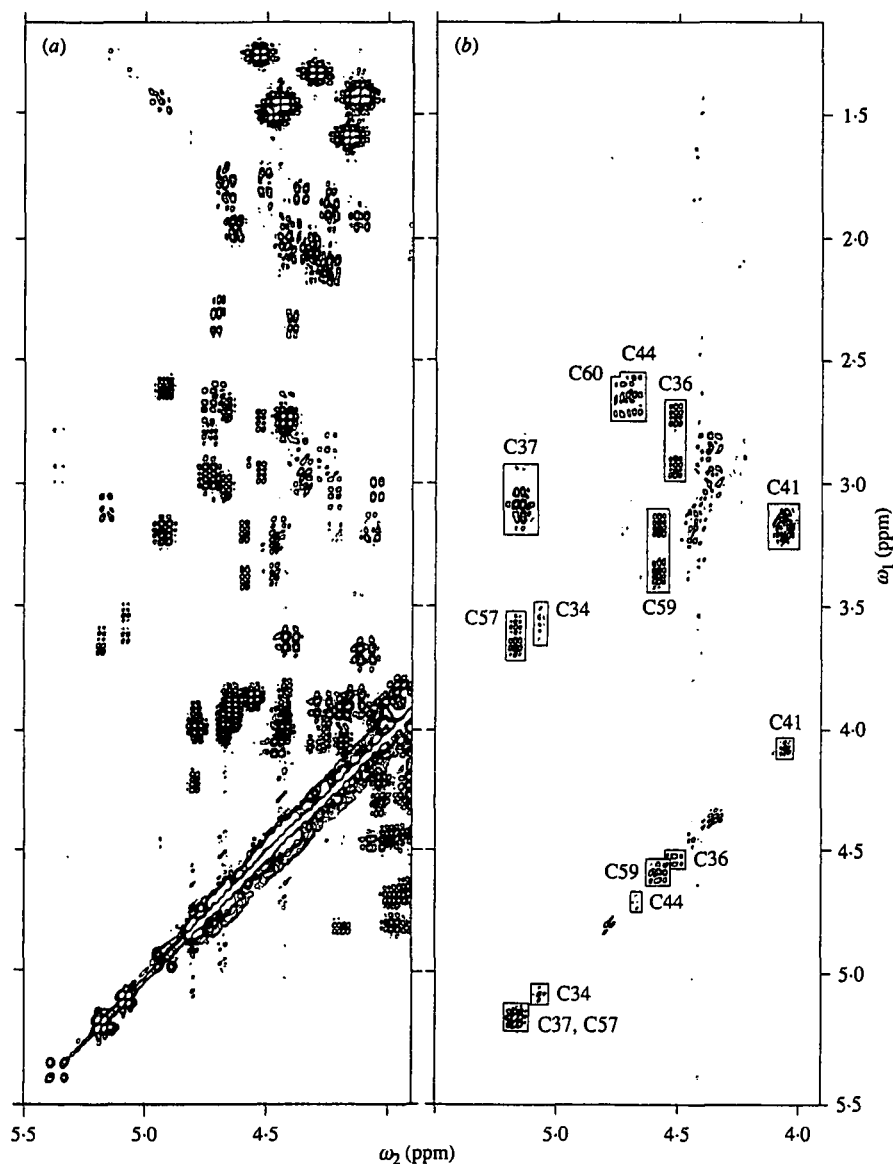
Fig. 4. (*a*) Conventional phase-sensitive [¹H,¹H]-COSY spectrum, and (*b*) difference spectrum from [¹H,¹H]-COSY with ¹¹³Cd-filter of rat [¹¹³Cd₇]-metallothionein-2 (D₂O, protein concentration 10 mM, 20 mM Tris buffer pD 7·0, 50 mM-KCl, 25 °C, ¹H frequency 360 MHz). The spectral region ($\omega_1 = 1\cdot1$–5·5 ppm, $\omega_2 = 3\cdot9$–5·5 ppm) is displayed, which contains the cross-peaks between Cᵅ-protons and Cᵝ-protons. In (*b*) the resonances originating from ¹¹³Cd-bound cysteines are framed and identified with the sequence positions. The diagonal peak at 4·75 ppm corresponds to the incompletely suppressed solvent resonance; the diagonal peaks and cross-peaks between $\omega_2 = 4\cdot35$ and 4·45 ppm correspond to additional Cys signals, which are not individually resolved. (From Wörgötter *et al.* 1988.)
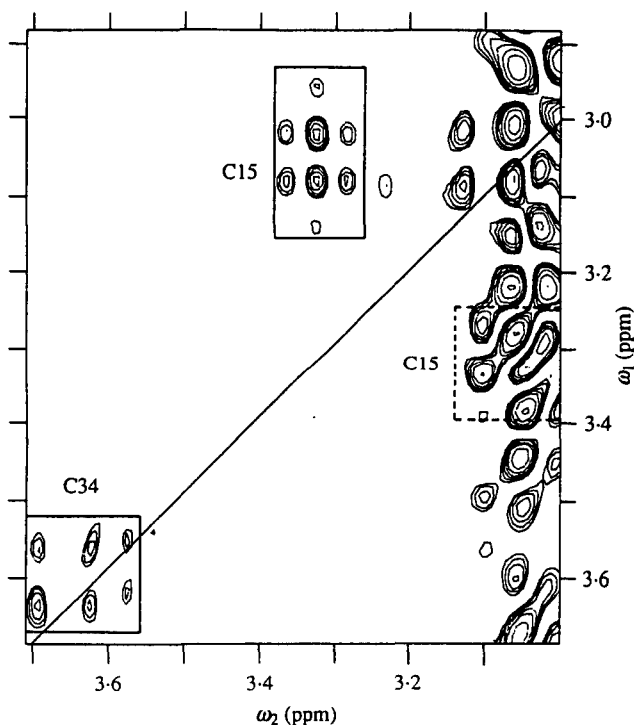
Fig. 5. Contour plot of the $H^{\beta2}-H^{\beta3}$ cross-peak region for cysteinyl side chains in rat metallothionein-2 from the difference spectrum of a $[^1H,^1H]$-COSY experiment with 2X-filter ($X = ^{113}Cd$; same experimental conditions as in Fig. 4). The position of the diagonal is indicated with a solid line. Resonances. originating from cysteines bound to two ^{113}Cd ions are framed and identified with the sequence positions. The band of t_1 noise at $\omega_2 = 3\cdot0-3\cdot1$ ppm stems from the $C^\varepsilon H_2$ resonances of Lys residues. (From Wörgötter *et al.* 1988.)

coupling constants $^4J(^1H,^{113}Cd)$. Fig. 5 shows the difference spectrum from a $[^1H,^1H]$-COSY with 2X-filter ($X = ^{113}Cd$) recorded with rat $[^{113}Cd_7]$-metallothionein. Eight of the total of 20 cysteinyl side chains in this protein are coordinated with two metal ions. The spectral region shown in Fig. 5 contains the $H^{\beta2}-H^{\beta3}$ cross-peaks of Cys15 and the diagonal peak of one of the C^β-protons of Cys34. Their presence in the 2X-filtered difference spectrum identifies these residues as bridging cysteines with resolved spin–spin couplings from the C^β-protons to two ^{113}Cd ions.

Overall, metallothionein is a good example of a problem where nX-filters are a powerful technique. Similar situations are presented quite generally by intermolecular interactions between hydrogen-bearing organic compounds and diamagnetic metal ions with a nuclear spin $I = \frac{1}{2}$. Although this appears to be a narrow area for potential applications, there is a large selection of bivalent metal-dependent enzymes and other proteins where the metal present in the native compound can be substituted by, for example, ^{113}Cd. DNA-binding Zn-finger proteins provide a good illustration (South *et al.* 1989). X-filter techniques might also be used for identification of less specific metal binding sites in proteins and

nucleic acids, possibly with ^{113}Cd as a 'NMR probe'. In all these potential applications the use of a nX-filter in the 2D [^{1}H,^{1}H]-NMR experiments would enable a characterization of the metal-binding sites with a single experiment recorded with the complex containing the NMR-active metal ion.

2.2 *nX-half-filters*

In biological macromolecules the one-bond coupling constants $^1\mathcal{J}(^1$H,^{15}N) and $^1\mathcal{J}(^1$H,^{13}C) are both large compared to all other homonuclear and heteronuclear coupling constants, and their variation among different ^{15}NH fragments, or different ^{13}CH fragments, respectively, is small (Bystrov, 1976). In work with isotope-labelled molecules, the X-half-filters can therefore be tuned for separating the diagonal peaks of X-bound protons and the cross-peaks with X-bound protons from all other peaks (Tables 1, 3). On this basis the combined use of isotope-labelling with ^{13}C or ^{15}N and 2D [^{1}H,^{1}H]-NMR with X-half-filters opens attractive ways to support both the determination of 3D protein structures and studies of intermolecular interactions with proteins and nucleic acids. As any given proton has only a single one-bond coupling constant with ^{13}C or ^{15}N, we limit the discussion to X-half-filters with $n = 1$.

We select the DNA-binding domain of the P22 c2 repressor (Fig. 6; Fig. 1 shows a [^{1}H,^{1}H]-NOESY spectrum of this protein in a complex with an operator DNA duplex) as an example to illustrate the use of [^{1}H,^{1}H]-NOESY with ^{15}N-half-filter in support of the determination of a three-dimensional protein structure. The spectra recorded with X-half-filters can be helpful on all three levels of data collection, i.e. for the resonance assignments, the identification of secondary structure elements, and the determination of the 3D structure (Wüthrich, 1986).

The feasibility of a protein structure determination by NMR depends primarily on one's ability to assign the ^{1}H-NMR spectrum (Wüthrich *et al.* 1982). Assignment of a protein ^{1}H-NMR spectrum includes the identification of the ^{1}H spin systems of the individual amino-acid residues, using through-bond, scalar spin–spin couplings. The spin systems are characteristic for the different amino-acid types, but since a protein usually contains multiple copies of any given amino acid (Fig. 6) the sequence positions cannot be determined from this information alone. Therefore, using through-space, dipolar couplings observed as ^{1}H–^{1}H NOEs, two or several sequentially neighbouring amino-acid spin systems are identified (*sequential assignments*). The peptide segments thus determined are then matched against the primary structure, and as a result the sequence-specific assignments are obtained. Clearly, the reliability of the sequential assignment procedure is reduced when all the amino-acid spin systems cannot be identified (Wüthrich, 1986). In the P22 c2 repressor individual identification of the ^{1}H spin systems of the long side chains of Leu, Glu, Gln, Met, Arg, Lys and Pro was difficult because of spectral overlap. In this situation, which can generally be anticipated for larger proteins and sometimes even for small proteins with unfavourable spectral properties, sequence-specific assignments were greatly facilitated by the identification of the Leu spin systems through ^{15}N-labelling and
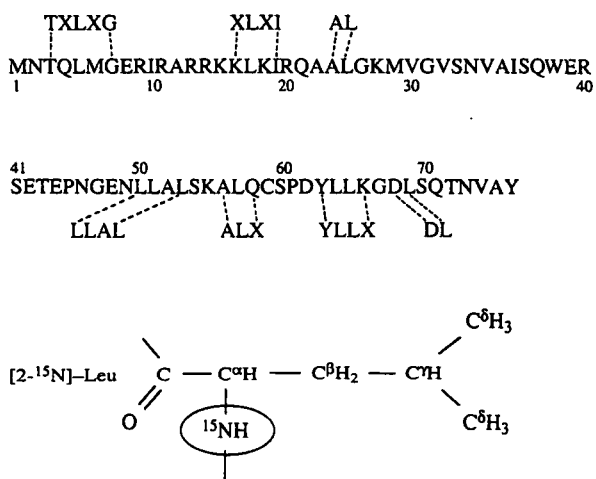
```
      TXLXG        XLXI   AL
MNTQLMGERIRARRKKLKIRQAALGKMVGVSNVAISQWER
1            10         20        30             40
```

```
41        50         60         70
SETEPNGENLLALSKALQCSPDYLLKGDLSQTNVAY
     LLAL        ALX       YLLX     DL
```

$$[2\text{-}^{15}\text{N}]\text{-Leu} \quad C - C^\alpha H - C^\beta H_2 - C^\gamma H \begin{matrix} C^\delta H_3 \\ \\ C^\delta H_3 \end{matrix}$$

Fig. 6. Amino-acid sequence of *Salmonella* phage P22 c2 repressor 1–76. The 10 Leu residues were labelled with ^{15}N in the extent of $> 85\%$. The letters above and below the sequence identify segments of neighbouring amino-acid spin systems in the primary structure, which were identified by sequential assignments with ^{1}H–^{1}H NOEs and led to sequence-specific assignments of all 10 leucines (see text). X stands for a residue from the group Glu, Gln, Met, Arg, Lys and Pro, for which the spin systems were not individually identified. At the bottom, the structure of ^{15}N-labelled Leu is shown.

the use of 2D [^{1}H,^{1}H]-NMR with X-half-filters. This is readily apparent from the following example: A tripeptide segment with three long amino acid side chains identified by sequential assignments in the non-labelled protein matches the six tripeptides 4–6, 13–15, 14–16, 15–17, 16–18, and 64–66 in the P22 c2 repressor sequence (Fig. 6). With the unique identification of the leucine spin systems by ^{15}N labelling the ambiguities of the sequence-specific assignments were greatly reduced, since only the two tripeptides 13–15 and 14–16 then contained three neighbouring residues with long side chains that had not been further specified (see Fig. 6).

Selective labelling of all 10 leucyl residues in P22 c2 repressor was achieved by growth of the *E. coli* overexpression system on a minimal medium containing ^{15}N-leucine, and the other amino acids in unlabelled form. Using a [^{1}H,^{1}H]-TOCSY experiment with ^{15}N(ω_2)-half-filter (Fig. 7) the ^{1}H resonance assignments for the amide protons and the C^α protons of the 10 leucyl residues were obtained (Otting *et al.* 1986). With these assignments, which were based entirely on covalent, scalar relations between the different nuclei, the [^{1}H,^{1}H]-NOESY spectrum with ^{15}N(ω_2)-half-filter was analysed. Fig. 8 shows the spectral region with the

Fig. 7. Difference spectrum from a [^{1}H,^{1}H]-TOCSY experiment with ^{15}N(ω_2)-half-filter of the DNA-binding domain 1–76 of P22 c2 repressor with all 10 leucyl residues labelled with ^{15}N (protein concentration 8 mM in H_2O, pH 4·8, $T = 20$ °C, MLEV-17 (Bax & Davis, 1985) was used during the mixing time of 60 ms, filter delay $\tau = 5\cdot5$ ms, $t_{1\,max} = 28$ ms, ^{1}H frequency 360 MHz). The multiplets are antiphase along ω_2. Positive and negative levels are plotted without distinction. (*a*) Spectral region ($\omega_1 = 6\cdot5$–$9\cdot3$ ppm, $\omega_2 = 6\cdot5$–$9\cdot3$ ppm). In a
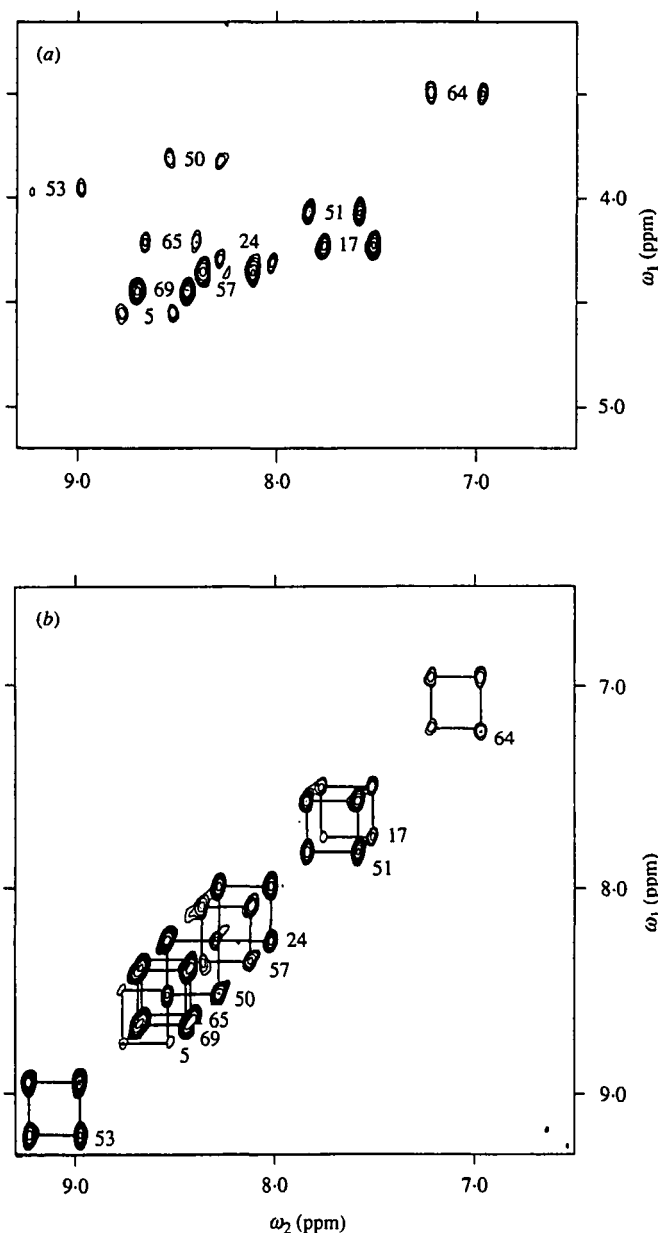
conventional [¹H,¹H]-TOCSY experiment this region contains the resonances of the amide protons and the aromatic protons. In the difference spectrum recorded with $^{15}N(\omega_2)$-half-filter all peaks have been suppressed except for the diagonal peaks originating from the ^{15}N-bound amide protons of Leu. The fine structure components of the diagonal peaks are connected by straight lines. (*b*) Spectral region (ω_1 = 3·1–5·2 ppm, ω_2 = 6·5–9·3 ppm). In conventional [¹H,¹H]-TOCSY this region contains the direct cross-peaks between the amide protons and the C^α-protons, and some relay peaks of Ser and Thr. In the difference spectrum recorded with $^{15}N(\omega_2)$-half-filter all peaks have been suppressed except for the direct cross-peaks between the amide protons and the C^α-protons of the ^{15}N-labelled leucines. In (*a*) and (*b*) the peaks of the Leu residues are identified with the sequence locations. (From Otting *et al.* 1986.)
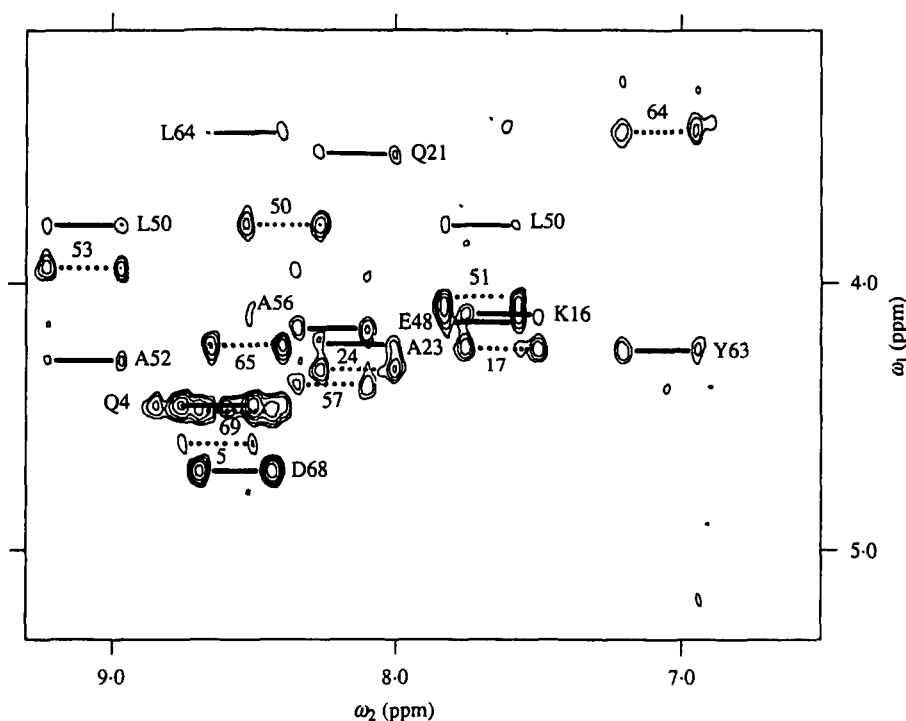
Fig. 8. Spectral region ($\omega_1 = 3\cdot1$–$5\cdot3$ ppm, $\omega_2 = 6\cdot6$–$9\cdot3$ ppm) of a NOESY spectrum with ^{15}N(ω_2)-half-filter recorded in a solution of P22 c2 repressor 1–76 in which all 10 leucyl residues were labelled with ^{15}N (Fig. 6; protein concentration 8 mM in H_2O, pH 4·8, 20 °C, mixing time = 100 ms, filter delay = 5·5 ms, $t_{1\,max}$ = 42 ms, ^{1}H frequency 360 MHz). The difference spectrum is shown. The multiplets are antiphase along ω_2. Positive and negative levels are plotted without distinction. The fine structure components of the cross-peaks are connected by horizontal lines. This spectral region contains NOEs between C^α-protons ($\omega_1 = 3\cdot1$–$5\cdot3$ ppm) and ^{15}N-labelled amide protons. Dotted lines identify the 10 intra-residual ^{15}NH–C^αH cross-peaks of the labelled leucyl residues. The cross-peaks from sequential and medium-range NOEs are identified by solid lines and labelled with the one-letter symbol and the sequence position of the unlabelled residue involved in the cross-peak. (From Senn *et al.* 1987*a*.)

C^αH–^{15}NH cross-peaks of the difference spectrum from a [^{1}H,^{1}H]-NOESY experiment with ^{15}N(ω_2)-half-filter. As the filter effect of the ^{15}N(ω_2)-half-filter is only active along the ω_2-frequency axis (Table 1), the difference spectrum contains all the cross peaks which connect the amide proton resonances of the 10 labelled leucines with the resonances of all protons that are close enough in space to give rise to a NOE with an amide proton of Leu. Although each cross-peak is split along ω_2 by the one-bond coupling constant $^1J(^1H,^1N)$, the spectrum is very much simplified when compared to the conventional NOESY spectrum recorded with the unlabelled protein (Fig. 1*b* gives an impression of the complexity of such spectra). In this spectral region the 10 intraresidual amide proton–C^α-proton cross-peaks of Leu (dotted lines) were readily identified, since they have the same chemical shifts in ω_1 and ω_2 as the corresponding direct connectivities in Fig. 7.

Next, sequential NOEs were identified in Fig. 8 and in other regions of the same spectrum, resulting in the identification of the peptide segments indicated in Fig. 6, and hence in the desired sequence-specific assignments for all 10 leucyl residues.

On the basis of the sequence-specific assignments the [^{1}H,^{1}H]-NOESY experiment with ^{15}N(ω_2)-half-filter provided direct information on the secondary polypeptide structure near several of the ^{15}N-labelled leucyl residues. For example, both Leu–Leu dipeptide segments (Fig. 6) were found to be located in α-helices, as evidenced by the strong sequential NOEs d_{NN} throughout the polypeptide segments 49–54 and 63–66 (not shown), and by the NOE connectivities $d_{\alpha N}$ (48, 51) and $d_{\alpha N}$ (50, 53) observed in Fig. 8 (Wüthrich *et al.* 1984). Similarly, several longer-range NOE cross-peaks with the leucyl amide protons could be detected in the simplified ^{15}N-half-filter spectra, which contributes further to the input for the calculation of the complete 3D structure (Wüthrich, 1986, 1989).

At present, and foreseeably also in the future, protein structure determination in solution will depend on the measurement of parameters that are accessible only with ^{1}H-NMR experiments (Wüthrich *et al.* 1982; Wüthrich, 1986). Supporting procedures using isotope-labelling and heteronuclear NMR techniques should therefore be designed primarily for the purpose of enabling easier access to ^{1}H-NMR data. This is exactly the function of heteronuclear filters. Thereby they have the special advantage of providing simplified ^{1}H-NMR spectra and other help in the spectral analysis without the need of ever having to record or assign the heteronuclear NMR spectrum.

The considerations on the use of heteronuclear half-filters for protein structure determination can readily be extended to complexes between two or several molecules. Consider, for example, a stable complex formed between a protein and a low-molecular-weight effector, or the interaction of a DNA fragment with a drug molecule. Assume further that the low-molecular-weight ligand molecule is fully labelled with ^{13}C. In such a system the observation in the [^{1}H,^{1}H]-NOESY spectra with ^{13}C-half-filter of the NOEs with the ^{13}C-bound protons may allow to identify the sites on the macromolecule that are in contact with the ligand, and to probe the local conformation around the ^{13}C-bound ligand protons. Foreseeably, studies of stable intermolecular complexes of isotope-labelled ligands with biological macromolecules could well turn out to be the most attractive use of heteronuclear half-filters (Fesik *et al.* 1988; Fesik, 1988).

2.3 *Heteronuclear half-filters and heteronuclear three-dimensional NMR*

The difference spectrum derived from a 2D [^{1}H,^{1}H]-NMR spectrum with X-half-filter represents the projection of a corresponding 3D X-correlated [^{1}H,^{1}H]-NMR data set (Fesik *et al.* 1989; Marion *et al.* 1989; Messerle *et al.* 1989) along the heteronuclear frequency axis onto a 2D plane with two proton frequency axes (Fig. 9). For example, in the three-dimensional versions of the ^{15}N-half-filter spectra of Figs 7 and 8, there would be 10 ω_1 (^{1}H)–ω_3(^{1}H)-planes at the 10 ^{15}N

(a)

(b)
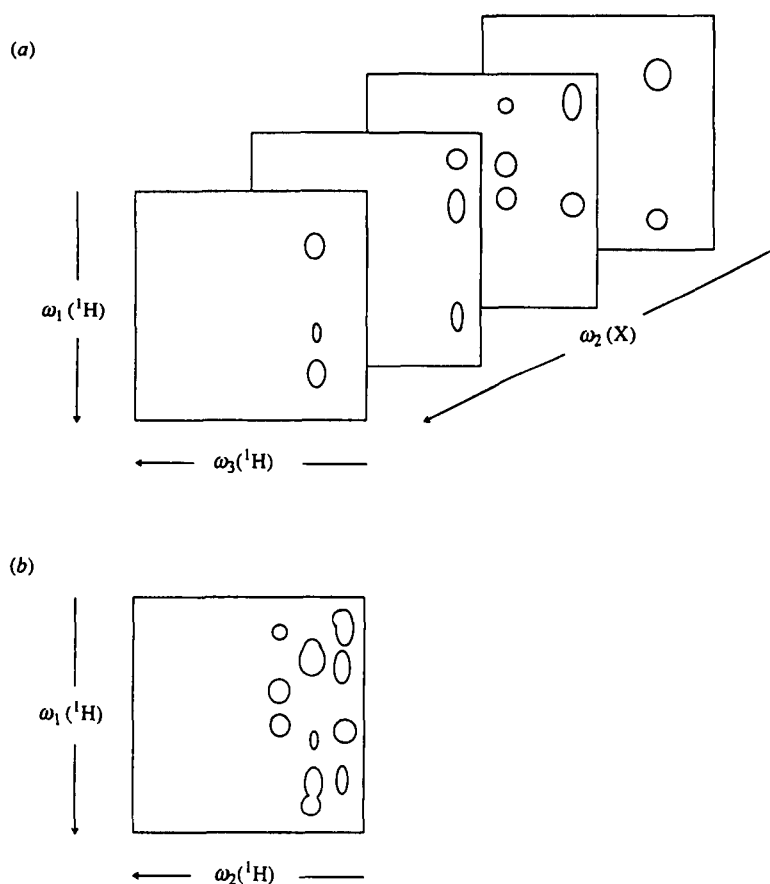
Fig. 9. Schematic presentation of a heteronuclear 3D NMR spectrum (*a*) and the corresponding $X(\omega_2)$-half-filtered 2D [^{1}H,^{1}H]-NMR experiment (*b*). (For example, these could be a 3D ^{15}N-correlated [^{1}H,^{1}H]-NOESY spectrum, and a 2D [^{1}H,^{1}H]-NOESY spectrum with ^{15}N(ω_2)-half-filter.) The spectrum (*b*) corresponds to a projection of the peaks in the different ω_1–ω_3 planes of spectrum (*a*) along the heteronuclear shift axis onto a single ω_1(^{1}H)–ω_3(^{1}H)-plane. (Note that the ω_3-axis of the 3D NMR spectrum corresponds to the ω_2-axis of the 2D NMR spectrum.)

chemical shifts of the leucyl residues in P22 c2 repressor. In the spectral region of the [^{1}H,^{1}H]-TOCSY spectrum shown in Fig. 7, each of these planes would contain a single cross-peak. In the 3D spectrum corresponding to Fig. 8, each plane would contain a linear array of cross-peaks at the ω_3 chemical shifts of the individual leucyl amide protons, and with variable ω_1 chemical shifts. This latter example would correspond to the scheme in Fig. 9.

Clearly, in the examples of Figs 7 and 8 the additional improvement of the spectral resolution afforded by the 3D experiment is not needed. In a *uniformly* ^{15}N-labelled protein, however, the spectral resolution of a [^{1}H,^{1}H]-NOESY experiment with ^{15}N-half-filter is usually only little improved relative to conventional [^{1}H,^{1}H]-NOESY, but further decisive improvements of the resolution can be achieved with the use of 3D NMR spectroscopy (Fesik *et al.* 1989). We conclude that any decision on the experiments to be used must be

tailored to the available isotope-labelling of the compounds studied. In each individual situation, the choice of the strategy to be used will depend primarily on the problem to be solved, but also on the efficiency of the procedures to be used and the financial expenditure. These general considerations indicate that the combinations of different types of selective isotope-labelling with heteronuclear half-filters in 2D [^{1}H,^{1}H]-NMR spectra, or random isotope-labelling with heteronuclear 3D NMR, respectively, will be valid alternatives in future practice.

3. FUNDAMENTAL CONSIDERATIONS ON HETERONUCLEAR FILTERS AND THEIR USE IN 2D [^{1}H,^{1}H]-NMR

3.1 *Hardware requirements*

2D [^{1}H,^{1}H]-NMR spectra with heteronuclear filters are obtained with experimental schemes consisting of pulses at the radiofrequencies of the protons and the heteronuclei, and of delays. These are combined with proper phase cycling of the pulses and the receiver to select the desired coherence transfer pathways. All these facilities are available in commercial multinuclear high-resolution NMR spectrometer systems. The sensitivity of proton observation can be optimized with the use of a reverse probehead, which has two separate radiofrequency coils. The inner coil is tuned and matched to the proton frequency, and is used for both the generation of ^{1}H radiofrequency pulses and for ^{1}H signal detection. The outer coil is selectively tuned and matched to the frequency of the heteronucleus of interest, and is used only to deliver radiofrequency pulses at the heteronuclear frequency. In a broadband probe one can choose from a wide range of heteronuclear frequencies, whereas a selective probe may be constructed for optimal performance with a single heteronucleus, for example, ^{15}N or ^{13}C.

3.2 *Product operator description of heteronuclear filtering*

In the product operator descriptions (Sørensen *et al.* 1983) of nX-filters we denote the heteronuclear spins as X, protons coupled to X as H, and protons not coupled to X as I. For X half-filters, X denotes again the heteronuclear spins, H designates X-bound protons with large one-bond couplings to which the filter delay is tuned, and I stands for protons that are not directly bound to a X nucleus. For simplicity of the presentation the calculations were performed for protons which are not coupled to any other protons and therefore give rise to diagonal peaks in the 2D [^{1}H,^{1}H]-NMR spectrum, and effects that might arise from spin relaxation and from strong spin–spin coupling are neglected.

  The effect of heteronuclear filters is based on the fact that the sign of proton magnetization in antiphase relative to a spin X can be inverted with the application of a π-pulse at the radiofrequency of X:

$$2H_x X_z \xrightarrow{\ (\pi)_x(X)\ } -2H_x X_z.$$

(1)

The combination of two experiments A and B with and without a $\pi(X)$-pulse then represents a straightforward means for separating the heteronuclear antiphase magnetization $2H_x X_z$ from in-phase proton magnetization I_x:

$$
\begin{aligned}
\text{experiment A: } I_x + 2H_x X_z &\xrightarrow{(\pi)_x(X)} I_x - 2H_x X_z, \\
\text{experiment B: } I_x + 2H_x X_z &\xrightarrow{} I_x + 2H_x X_z.
\end{aligned}
\qquad (2)
$$
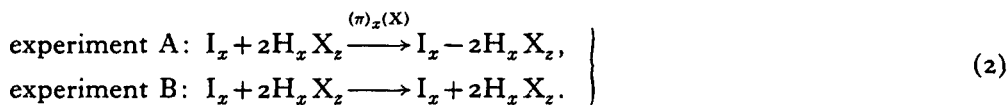
Two linear combinations of A and B yield the desired subspectra: The difference of the two data sets obtained from the experiments A and B selects the term $2H_x X_z$, while the sum contains the proton magnetization I_x.

The $\pi(X)$-pulse which is inserted to achieve the subspectral editing is called the *editing pulse*. In practice the presence of a $\pi(X)$-pulse in experiment A and its absence in experiment B are achieved by the combination of two $(\pi/2)(X)$-pulses,

$$
(\pi/2)_x(X) - (\pi/2)_\psi(X).
\qquad (3)
$$

The phase of the first pulse in (3) is kept constant, and the $(\pi/2)_\psi(X)$-pulse is actually the editing pulse. An effective $(\pi)_x(X)$-pulse is obtained with $\psi = x$, and an effective zero degree pulse with $\psi = -x$. This scheme ensures that the same pulse power is used in both experiments, and it minimizes potential artefacts that might arise from combining two data sets recorded under non-identical conditions (Freeman *et al.* 1981).

With the phase cycle of a *n*-quantum filter (Piantini *et al.* 1982), the pair of $(\pi/2)(X)$-pulses [equation (3)] can be used to select proton coherences which are antiphase with respect to n heterospins X (Wörgötter *et al.* 1988). For example, to select the coherences with an even number of X operators in the product operator representation, e.g. $4H_x X_z X_z'$, the phase of the first $(\pi/2)(X)$-pulse is kept constant, while the phase ψ of the second, editing $(\pi/2)(X)$-pulse is cycled through x, y, $-x$, and $-y$. The data sets recorded with the phases x and $-x$, and those recorded with y and $-y$, respectively, are stored separately. Their summation and subtraction result in the sum spectrum and the difference spectrum, respectively. The signals in the difference spectrum come from those coherences which have passed the 2X-filter.

The most straightforward application of the pair of pulses in equation (3) for subspectral editing is realized with the nX-filters. nX-half-filter techniques use the pulse combination of equation (3) together with a filter delay.

3.3 *Extension of 2D [^{1}H,^{1}H]-NMR experiments with heteronuclear filters*

Heteronuclear filters can be inserted into any 2D [^{1}H,^{1}H]-NMR pulse scheme. In the phase cycling program of the resulting experiment with heteronuclear filter, the phase cycle of the basic [^{1}H,^{1}H]-NMR experiment is retained and has to be extended by independent phase cycling of the additional pulses introduced by the heteronuclear filter. The total number of steps in the resulting overall phase cycle corresponds to the product of the number of phase cycling steps in the basic ^{1}H-NMR experiment and those in the heteronuclear filter.

For practical purposes, if complete phase cycling is attempted the phase cycling schemes of 2D [^{1}H,^{1}H]-NMR experiments with heteronuclear filters may result in unacceptably long measuring times. This is best illustrated with a numerical example corresponding to a typical experiment with a biological macromolecule: 500 free induction decays must be acquired to record a phase-sensitive 2D NMR data set that covers a sweep width of 10 ppm at 500 MHz with a maximum evolution time, $t_{1 \, max}$, of 50 ms. For an experiment with a 64-step phase cycle and a repetition rate of 1·4 s per scan, the total measuring time is at least $500 \times 64 \times 1·4 \, s \approx 12$ h. Experiments with n-fold longer phase cycles require n times longer measuring times. All the individual steps in the complete, 'optimal' phase cycling schemes for 2D [^{1}H,^{1}H]-NMR experiments do, however, not have equal weight, and some steps may be omitted without causing major deterioration of the quality of the resulting spectra. In the descriptions of individual experiments with heteronuclear filters (sections 4–6 below), a sequence of phase cycling priorities is indicated with each of the experimental schemes. These priority lists indicate the order in which the individual 2-step phase cycles should preferably be applied. Only minor artefacts are expected to result from omission of steps given at the end of the priority list, whereas the phase cycling steps at the top of the list are indispensible for obtaining spectra of satisfactory quality.

As an illustration of these somewhat abstract comments on phase cycling in 2D [^{1}H,^{1}H]-NMR with heteronuclear filters, the following subsections 3.3.1–3.3.3 describe, respectively, phase-cycling schemes that have proven to produce high-quality spectra with the conventional [^{1}H,^{1}H]-COSY and [^{1}H,^{1}H]-NOESY experiments, and a discussion of two alternative priority lists for phase cycling with the heteronuclear filters. Considerations similar to those described for COSY and NOESY apply for other 2D [^{1}H,^{1}H]-NMR experiments, which can all be supplemented with heteronuclear filters.

3.3.1 *Phase-cycling in the [^{1}H,^{1}H]-COSY experiment*

The experimental scheme of phase-sensitive COSY is shown in Fig. 10*a* together with the coherence transfer pathway selected by the standard phase cycling for this experiment (Bodenhausen *et al.* 1984). The experiment consists of two ($\pi/2$) pulses with phases ϕ_1 and ϕ_2, which are separated by the evolution period t_1 and succeeded by the detection period t_2 (Aue *et al.* 1976; Ernst *et al.* 1987; Wüthrich, 1986). For each t_1 value the experiment is repeated eight times with different phase settings of the radio frequency pulses and the receiver. These eight phase settings are listed in Fig. 10*b*. To further improve the signal-to-noise ratio, the entire phase cycle may be repeated n times with accumulation of a total of 8n scans.

The phase cycling of Fig. 10*b* contains the three basic 2-step cycles of Fig. 10(*c–e*). In step (*c*) the simultaneous incrementation of the phases of the two pulses and the receiver from x to y ensures the elimination of undesired quadrature images. (A quadrature image originating from unbalanced receiver channels in dual channel detection would lead to an anti-diagonal in the 2D [^{1}H,^{1}H]-NMR spectrum). The phase cycle of Fig. 10*c* corresponds only to the

(*a*)
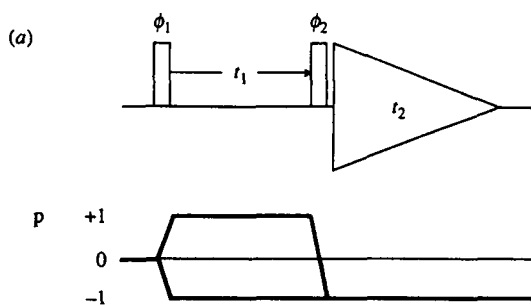
(*b*) $\phi_1 = x$ y x y $-x$ $-y$ $-x$ $-y$

$\phi_2 = x$ y $-x$ $-y$ x y $-x$ $-y$

rec $= x$ y x y $-x$ $-y$ $-x$ $-y$

(*c*) $\phi_1 = x$ y (*d*) $\phi_1 = x$ $-x$ (*e*) $\phi_1 = x$ $-x$

$\phi_2 = x$ y $\phi_2 = x$ $-x$ $\phi_2 = x$ x

rec $= x$ y rec $= x$ x rec $= x$ $-x$

Fig. 10. (*a*) Experimental scheme of phase-sensitive [^{1}H,^{1}H]-COSY. The two vertical bars represent $\pi/2$ radiofrequency pulses. (The experimental schemes discussed in this review contain exclusively pulses of duration $\pi/2$ or π. These two pulse lengths are distinguished by the thickness of the bars. The phases of the pulses are indicated above the pulse symbols). t_1 is the evolution period. The triangle represents the free induction decay during the detection period t_2. To obtain a 2D data set $s(t_1,t_2)$, the experiment is repeated with incrementation of t_1, typically for about 512 t_1 values. For each t_1 value multiple scans are accumulated to improve the signal-to-noise ratio. During this accumulation the phases of the pulses and the receiver (rec) are cycled. The minimal number of scans for each t_1 value is thus determined by the length of the phase cycle used. The coherence transfer pathway selected by the phase cycle (*b*) is indicated below the pulse sequence, where p is the order of coherence. (*b*) Complete 8-step phase cycle used to obtain the coherence transfer pathway in (*a*) and to suppress unwanted quadrature images. (*c*) Phase cycle of 2-step CYCLOPS. (*d*), (*e*) Basic two-step phase cycles for the selection of the coherence transfer pathway.

first half of the conventional CYCLOPS phase cycle (Hoult & Richards, 1975) and will in the following be referred to as 2-*step CYCLOPS*. In the complete CYCLOPS phase cycle, simultaneous incrementation of the phases of all pulses and the receiver in steps of 90° or 120° (Hoult & Richards, 1975; Bodenhausen *et al.* 1984) results in the suppression of DC-offsets (DC = direct current) in the free induction decays, in addition to the quadrature image suppression. The use of 2-step CYCLOPS is a compromise resulting in a 2-fold reduction of the length of the overall phase cycle, which will be of practical interest for the experiments with heteronuclear filters. The absence of DC-offset suppression is acceptable, as is shown by the following considerations: The Fourier transform of a DC-offset is a spike at the carrier frequency, which will give rise to a narrow band of t_1 noise. This t_1 noise band at the carrier frequency of the 2D spectrum is negligibly weak compared to the t_1 noise from the water signal. Therefore, if in experiments

recorded in aqueous solution the radiofrequency carrier is placed at the frequency of the solvent resonance, this artefact will hardly be noticeable. It is further worth noting that the elimination of quadrature images by 2-step CYCLOPS depends critically on the reproducibility of the experimental conditions during the time period between the two steps of the phase cycle. Therefore, it is advisable to apply 2-step CYCLOPS before the cycling of the other phases. The two additional 2-step phase cycles of Fig. 10(d, e) select for the coherence transfer pathway indicated below the pulse sequence in Fig. 10a.

The complete COSY phase cycle of Fig. 10b was generated by independent cycling of each of the steps of Fig. 10$(c-e)$. Thus, the first two steps of the COSY phase cycle correspond to 2-step CYCLOPS (Fig. 10c). The next two steps are obtained by repetition of the first two steps, but with alternation of the phase ϕ_2 according to Fig. 10d. Finally, the first four steps are repeated with simultaneous phase alternation for the first pulse and the receiver (Fig. 10e). The sequence in which the basic 2-step phase cycle elements are used in Fig. 10b corresponds to the phase cycle priority list: 2-step CYCLOPS, ϕ_2, ϕ_1.

3.3.2 *Phase cycling in the [^{1}H,^{1}H]-NOESY experiment*

Fig. 11a shows the experimental scheme of a NOESY experiment. Three ($\pi/2$) pulses with phases ϕ_1, ϕ_2 and ϕ_3 are separated by the evolution period t_1 and the mixing period τ_m, and succeeded by the detection period t_2. Fig. 11b shows the phase cycling suggested for use in experiments with heteronuclear filters. As with COSY, 2-step CYCLOPS is used to shorten the phase cycle. Another compromise accepted with this scheme is that in contrast to the routinely used, more extensive phase cycle for NOESY (Bodenhausen *et al.* 1984), the present version does not suppress two-quantum coherence (Macura *et al.* 1981).

The phase cycle in Fig. 11b has been generated along similar lines as the aforementioned COSY phase cycle of Fig. 10b. The individual 2-step phase cycles are shown in Fig. 11$(c-f)$. 2-step CYCLOPS (Fig. 11c) is again used for quadrature image suppression. The overall phase program of Fig. 11b is obtained by additional independent alternation of the phases ϕ_3 (Fig. 11d), ϕ_2 (Fig. 11e) and ϕ_1 (Fig. 11f) with simultaneous alternation of the receiver phase. The coherence transfer pathway selected by this simple alternation of the phases ϕ_1, ϕ_2 and ϕ_3 eliminates single quantum coherence during the mixing period.

3.3.3 *Two alternative priority lists for the phase cycling in 2D [^{1}H,^{1}H]-NMR with heteronuclear filters*

As was mentioned at the outset of section 3.3, phase-cycling priority lists will be indicated with each individual experiment described in sections 4–6. Here, we discuss two alternative phase-cycling schemes. The choice between the two schemes will depend primarily on the overall measuring time available. In principle it is desirable to cycle the phase of the editing ($\pi/2$)(X)-pulse [see equation (3)] first. This ensures that the data sets recorded with different phases of the editing pulse are not significantly affected by spectrometer instabilities,
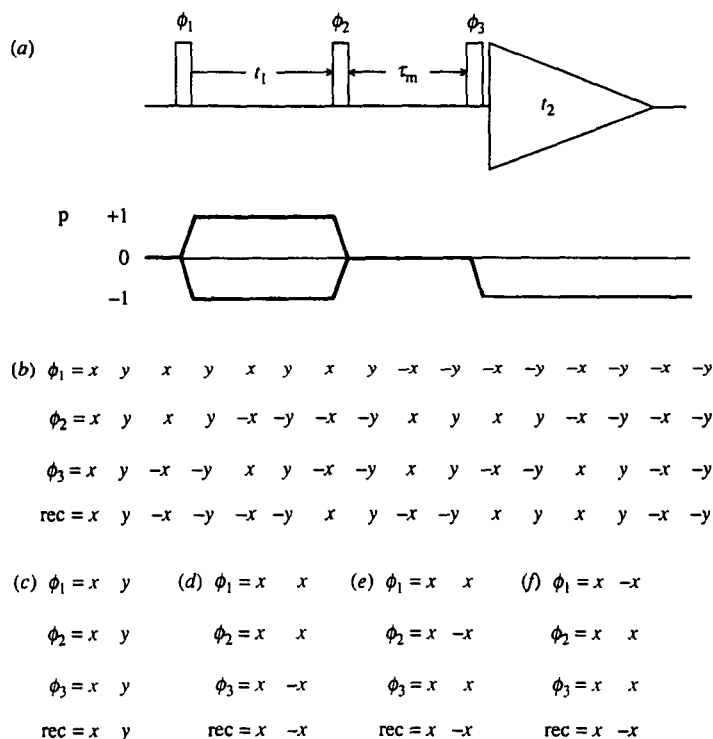
Fig. 11. (a) Experimental scheme of phase-sensitive [^{1}H,^{1}H]-NOESY. τ_m is the mixing time. The coherence transfer pathway selected by the phase cycle (b) is indicated below the pulse sequence. (b) Complete 16-step phase cycle used to obtain the coherence transfer pathway in (a) and to suppress unwanted quadrature images. (c) Phase cycle of 2-step CYCLOPS. (d)–(f) Basic two-step phase cycles for the selection of the coherence transfer pathway.

which might contribute to deterioration of the result of their later summation or subtraction. However, in turn one then has to consider that coherent artefacts from insufficient relaxation between successive scans can accumulate if each scan for the data set with effective $\pi(X)$-editing pulse is always immediately followed by the corresponding scan for the data set without effective editing pulse. It has been shown by Wörgötter *et al.* (1988) that these artefacts can be suppressed by repetition of the phase cycle with permuted order of the phase of the editing $(\pi/2)(X)$-pulse. In the first half of this extended phase cycle, each scan for data set A is followed by the corresponding scan for data set B [equation (2)], while in the second half the scans for data set A are sampled after the corresponding scans for data set B. In the following this procedure will be referred to as 'repetition of the phase cycle with permuted order of the phase ψ of the editing $(\pi/2)(X)$-pulse'. For experiments with 2X-filters or 2X-half-filters a 4-fold permutation of the phase cycle has been recommended (Wörgötter *et al.* 1988).

Inevitably the repetition of the phase cycle with permuted order of ψ doubles the overall length of the phase cycle. In situations where this is not acceptable, an alternative phase-cycling priority list is recommended, with the phase ψ of the editing pulse as the last step rather than the first step. This alternative data collection scheme imposes more stringent requirements on the stability of the
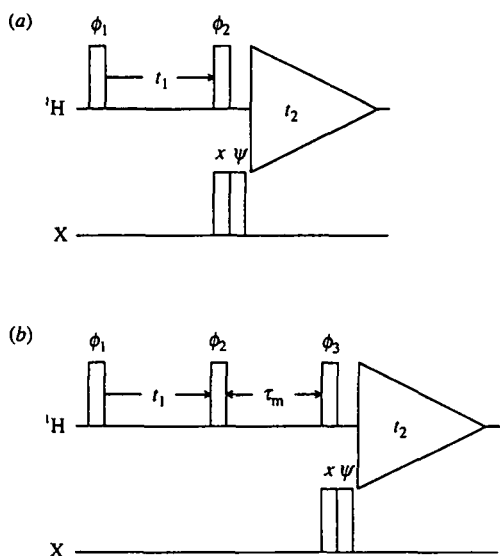
Fig. 12. Experimental schemes for (a) [^{1}H,^{1}H]-COSY with X-filter, and (b) [^{1}H,^{1}H]-NOESY with X-filter. The letters ^{1}H and X, respectively, identify the entries for pulses and delays at the radiofrequencies of the protons and the heteronucleus.

spectrometer, but it avoids the bias in the data from insufficient relaxation between successive scans. A further reduction of this bias can be achieved, if two to four dummy scans are inserted between the sets of scans recorded with different phases of ψ. These two alternative phase cycling schemes are further discussed in section 7 below.

4. 2D [^{1}H,^{1}H]-NMR EXPERIMENTS WITH nX-FILTERS

4.1 *Product operator description of X-filters in* [^{1}H,^{1}H]*-COSY and* [^{1}H,^{1}H]*-NOESY*

In 2D [^{1}H,^{1}H]-NMR experiments with X-filter the pair of $(\pi/2)(X)$-pulses is inserted during the mixing period (Wörgötter *et al.* 1986). Fig. 12 shows the resulting experimental schemes of [^{1}H,^{1}H]-COSY and [^{1}H,^{1}H]-NOESY with X-filter. The phase cycles of the proton pulses are the same as for the corresponding unfiltered experiments (Figs 10, 11). The phase-cycle priority list for COSY with X-filter is: ψ, 2-step CYCLOPS, ϕ_2, ϕ_1, and repetition with permuted order of ψ. This leads to a 32-step phase cycle. For NOESY with X-filter we have the phase cycling priority list: ψ, 2-step CYCLOPS, ϕ_3, ϕ_2, ϕ_1, and repetition with permuted order of ψ. This results in a 64-step phase cycle.

Following equations (2) and (3), the data sets recorded with phases x and $-x$ of the editing $(\pi/2)_\psi(X)$-pulse are stored separately. The difference spectrum obtained by subtraction of these two data sets (Tables 1 and 2) contains only peaks from proton resonances that have evolved into antiphase magnetization with respect to the heteronucleus X during the evolution period t_1, and are therefore sensitive to the editing pulse. During the detection period t_2 they refocus into observable in-phase magnetization. If the proton coherence is transferred from a

X-coupled proton to other protons by the mixing scheme used in the 2D [^{1}H,^{1}H]-NMR experiment, the resulting coherence is still antiphase with respect to the X-spin, and will become observable during t_2 only if these other protons also have non-vanishing scalar couplings to the heterospin. Therefore, the difference spectrum contains exclusively cross peaks between pairs of protons which are *both* coupled to the *same* heteronucleus X (Tables 1, 2). In the sum spectrum obtained by addition of the two data sets recorded with $\psi = x$ and $-x$, respectively, the observed peaks result from those product operator terms which are insensitive to the phase of the editing pulse.

Starting from equilibrium magnetization of a proton coupled to a X spin, H_z, and a proton not coupled to X, I_z, the product operator calculation shows that the following terms are created at the start of the detection period:

[^{1}H,^{1}H]-COSY with X-filter

$$H_z \xrightarrow{\hspace{3cm}} \sin \Omega t_1 \cos \pi \mathcal{J}_{HX} t_1 H_x \mp \cos \Omega t_1 \sin \pi \mathcal{J}_{HX} t_1 2H_x X_z \left.\vphantom{\begin{matrix}a\\b\end{matrix}}\right\} \quad (4)$$
$$I_z \xrightarrow{\hspace{3cm}} \sin \Omega t_1 I_x .$$

[^{1}H,^{1}H]-NOESY with X-filter

$$H_z \xrightarrow{\hspace{3cm}} \cos \Omega t_1 \cos \pi \mathcal{J}_{HX} t_1 H_y \pm \sin \Omega t_1 \sin \pi \mathcal{J}_{HX} t_1 2H_y X_z \left.\vphantom{\begin{matrix}a\\b\end{matrix}}\right\} \quad (5)$$
$$I_z \xrightarrow{\hspace{3cm}} \cos \Omega t_1 I_y .$$

The trigonometric coefficients depending on Ωt_1 and $\mathcal{J}_{HX} t_1$ describe the evolution of the magnetization under the chemical shift Hamiltonian and under scalar coupling, respectively, during the evolution time t_1 (Sørensen *et al.* 1983). As in all product operator calculations in this text, only the coherence transfer pathway selected by the phase cycling used (see Figs 10, 11) has been taken into account in equations (4) and (5). The upper and lower signs in equations (4) and (5) correspond, respectively, to the phase settings $\psi = X$ and $\psi = -X$ of the editing $(\pi/2)(X)$-pulse. The difference between the two data sets recorded with different phase ψ of the editing $(\pi/2)(X)$-pulse selects the terms $2H_x X_z$ [equation (4)] and $2H_y X_z$ [equation (5)], respectively, whereas the sum contains all in-phase magnetization. The X-coupled proton spins H occur in the two subspectra with different multiplet fine structures. Thus the X-filter is a technique for editing the multiplet fine structure of X-bound protons (rather than complete cross-peaks or complete diagonal peaks) into different subspectra. Nonetheless, since the proton spins I are absent from the difference spectrum, this subspectrum may be considerably simplified for suitably isotope-labelled compounds (Fig. 4). In contrast, the sum spectrum contains all the peaks seen in the conventional 2D [^{1}H,^{1}H]-NMR experiment (Table 1).

The product operator terms of equations [4] and [5] give an accurate description of the phases and the multiplet fine structures observed in the X-filtered experiments. The trigonometric factors contain the phase and multiplet information for the t_1 domain, and the operator terms contain the corresponding information about the t_2 domain. We thus see that the sum spectrum and the difference spectrum have the same phase in both dimensions: In the COSY experiment the trigonometric factors are all odd and the transverse operator terms are all along the x-axis. In the NOESY experiment the trigonometric factors are all even and the transverse operator terms are all along the y-axis. For all

multiplets the fine structure in the sum spectrum is in-phase with respect to the X spin in both dimensions, because the functional dependence on $\mathcal{J}_{HX}t_1$ is cosine modulated and the operator terms represent in-phase magnetization. In contrast, since the functional dependence on $\mathcal{J}_{HX}t_1$ is sine modulated and the product operator terms are antiphase with respect to the heteronucleus X, the peaks in the difference spectrum are antiphase in both dimensions with respect to the heteronuclear coupling $\mathcal{J}_{HX}$. (Note that these heteronuclear antiphase multiplets cannot be decoupled with heteronuclear broadband decoupling.) The corresponding conventional 2D [^{1}H,^{1}H]-NMR spectrum without X-filter can be thought of as the sum of the two subspectra obtained with the X-filter. For example, in NOESY [equation (5)] the diagonal peaks of X-bound protons would be represented by the superposition of the in-phase multiplet $\cos \Omega t_1 \cos \pi \mathcal{J}_{HX}t_1 H_y$ with the antiphase multiplet $-\sin \Omega t_1 \sin \pi \mathcal{J}_{HX}t_1 2H_yX_z$. Only half of the multiplet components are thus observed in the standard 2D [^{1}H,^{1}H]-NMR spectra of X-coupled protons, and the resulting multiplet pattern is of E. COSY-type (Griesinger *et al.* 1986) with respect to the heteronuclear coupling. (This phenomenon was initially observed and analyzed in [^{1}H,^{1}H]-COSY spectra of [^{113}Cd$_7$]-metallothionein (Neuhaus *et al.* 1984)).

4.2 *Experimental examples of [^{1}H,^{1}H]-COSY and [^{1}H,^{1}H]-NOESY with X-filters*

A practical application of [^{1}H,^{1}H]-COSY with X-filter is presented in Fig. 4, and Fig. 5 illustrates the use of a 2X-filter. In these experiments with the protein [^{113}Cd$_7$]-metallothionein, the identification of ^{113}Cd-coupled protons was based on the presence of the corresponding signals in the simplified difference spectra.

An experimental verification of the quantitative predictions on the multiplet fine structures in 2D [^{1}H,^{1}H]-NMR experiments with or without X-filter [equations (4) and (5)] was obtained with an experiment recorded with a sample of ^{113}Cd^{2+}-EDTA using the experimental scheme of Fig. 12b. The cross-peak shown in Fig. 13 manifests a NOE between two methylene protons, H and H', which are also coupled to each other via the scalar coupling constant $\mathcal{J}_{HH'}$. In addition, both protons have non-vanishing heteronuclear coupling constants, $\mathcal{J}_{HX}$ and $\mathcal{J}_{H'X}$, with the ^{113}Cd ion. The 1D multiplet pattern of each proton is a doublet of doublets (Fig. 13a, top panel). Equation (5) can be expanded to describe the multiplet fine structure of the NOESY cross-peaks of Fig. 13 by multiplication of each term on the right by the factor $\cos \pi \mathcal{J}_{HH'}t_1$, which describes the scalar coupling between the two methylene protons. The proton–proton coupling $\mathcal{J}_{HH'}$ causes a splitting of the cross-peak multiplet into four components centred on the corners of a square spanned by the coupling constant $\mathcal{J}_{HH'}$ (see the top panel of Fig. 13a). Fig. 13a shows the E. COSY-type cross-peak pattern observed in an unfiltered [^{1}H,^{1}H]-NOESY experiment, which corresponds to the data set recorded with $\psi = -x$ (Fig. 12b). Fig. 13b shows the result obtained with $\psi = x$. The difference and the sum of the data of Fig. 13(a, b), are shown in Fig. 13(c, d). The overall absolute intensity of the fine structure components in the cross-peak of Fig. 13(c, d), is the same as in the corresponding unfiltered experiment of
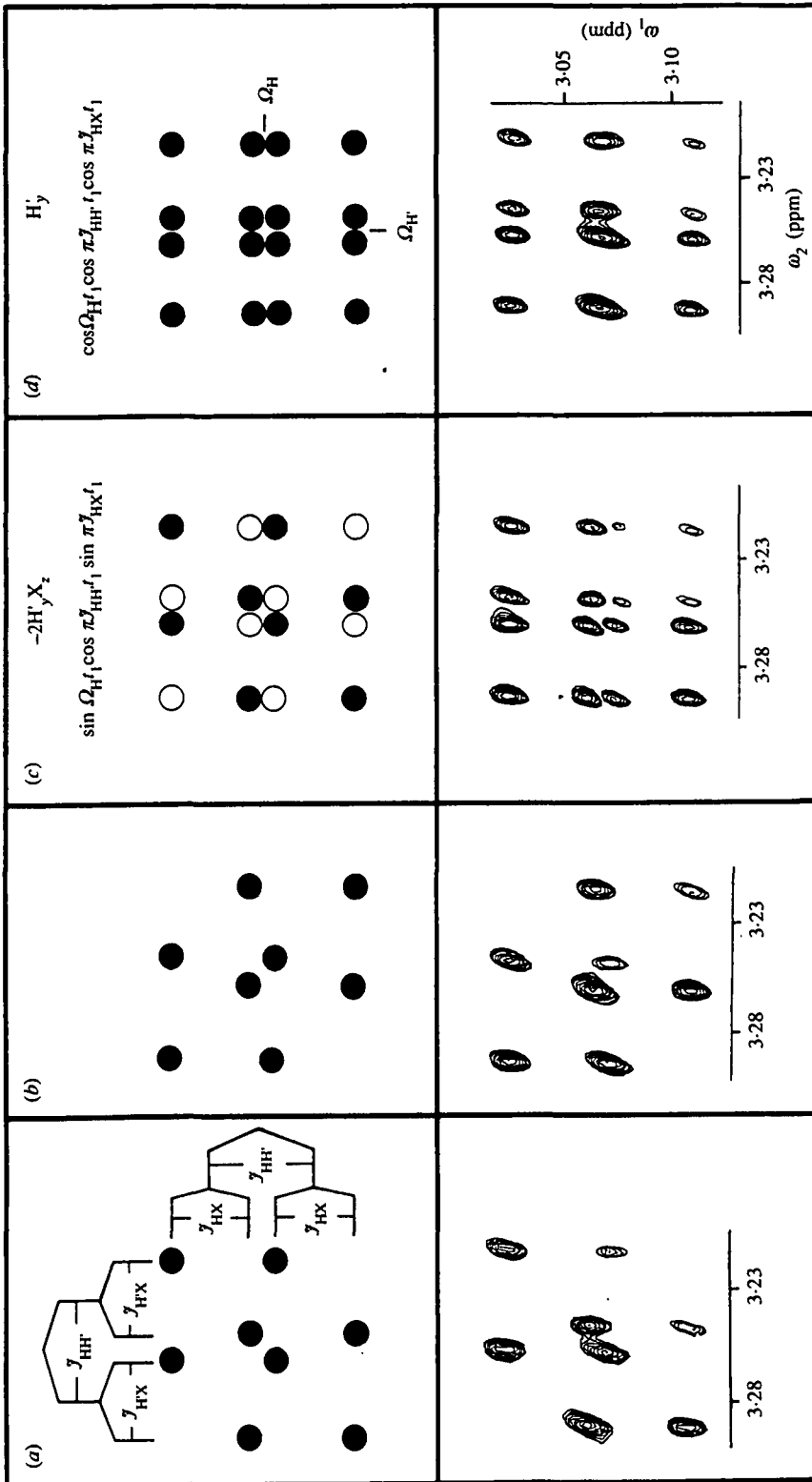
Fig. 13. For legend see opposite page.

Fig. 13 a. However, in the X-filtered spectra the intensity is distributed among twice the number of multiplet components, so that the intensity of each individual component is halved.

5. 2D [^{1}H,^{1}H]-NMR EXPERIMENTS WITH X-HALF-FILTERS

For reasons outlined at the outset of section 2.2 the following treatment is limited to X-half-filters, although higher order nX-half-filters with $n > 1$ can in principle also be devised.

5.1 *X-half-filter elements*

The basic X-half-filter element (Otting *et al.* 1986) is shown in Fig. 14 a. It consists of a filter delay of duration $\tau = 1/2 \mathcal{J}_{HX}$, where $\mathcal{J}_{HX}$ is the heteronuclear coupling constant recognized by the filter, and of pulses on both the proton channel and the heteronuclear channel. The $\pi(^1$H)-pulse in the centre of the delay refocuses the chemical shift evolution of the protons. The phase ζ of the $\pi(^1$H)-pulse is alternated between x and $-x$ to compensate for deviations from the 180° flip angle and for off-resonance effects (Fig. 14 d; Bodenhausen *et al.* 1977). The receiver phase is kept constant upon alternation of the phase ζ (Fig. 14 d). The phase ψ of the last, editing $(\pi/2)(X)$-pulse is alternated between x and $-x$ independently of the phase ζ. Its combined effect with the preceding $(\pi/2)_x(X)$-pulse is that of an effective $(\pi)_x(X)$-pulse for $\psi = x$, or a zero degree pulse for $\psi = -x$. The receiver phase is not changed upon alternation of the phase ψ, but the data recorded with $\psi = x$ and $\psi = -x$ are stored in different memory locations, so that they can be additively or subtractively combined after the recording of the complete data set to yield the desired subspectra (Table 1).

To describe the X-half-filter in terms of product operators we make use of the fact that the one-bond coupling constants $^1\mathcal{J}(^1$H,X) between X and the directly bonded protons are nearly identical for all fragments H–X, and are much larger than any other homonuclear or heteronuclear coupling constant involving the

---

Fig. 13. Comparison of the experimental multiplet patterns (bottom) of the NOESY cross-peak connecting the acetate methylene protons H and H' in ^{113}Cd^{2+}-EDTA (ethylenediaminetetraacetate) with the pattern predicted for an HH'X spin system with $|\mathcal{J}_{HH'}| = 16\cdot5$, $|\mathcal{J}_{HX}| = 13\cdot6$, and $|\mathcal{J}_{H'X}| = 12\cdot0$ Hz (top part of the figure). In the predicted spectra full and open circles indicate opposite signs of the multiplet components. (a) [^{1}H,^{1}H]-NOESY. The analysis in terms of spin–spin coupling constants is indicated in the predicted spectrum. (b) [^{1}H,^{1}H]-NOESY with an effective $\pi(^{113}$Cd)-pulse applied simultaneously with the ^{1}H observation pulse (Fig. 12 b). (c) Difference spectrum from [^{1}H,^{1}H]-NOESY recorded with a ^{113}Cd filter. In the experiment the signs of the individual fine structure components coincide with those predicted. The product operator expression for this cross-peak is given at the top. It can be derived from the second product operator term for X-coupled protons in equation (5), which describes the diagonal peaks, by multiplication with a factor accounting for the homonuclear scalar coupling between the two NOE-related protons H and H', $\cos \pi \mathcal{J}_{HH'} \cdot t_1$. (d) Sum spectrum from [^{1}H,^{1}H]-NOESY recorded with a ^{113}Cd filter. The product operator description for this cross peak can be derived from the first product operator term for X-coupled protons in equation (5). (From Wörgötter *et al.* 1986.)

3-2
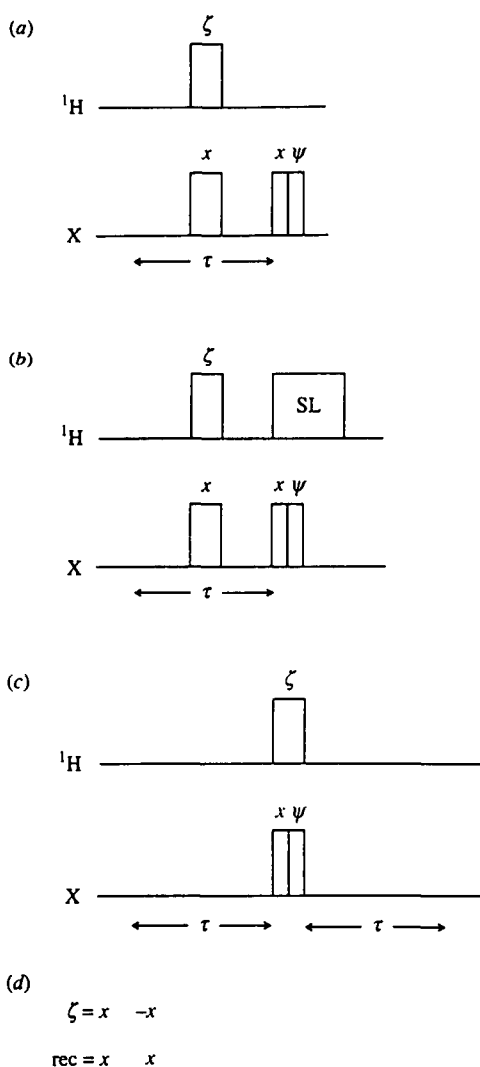
Fig. 14. X-half-filter elements. The filter delay τ is optimally tuned with $\tau = 1/2J_{HX}$. The $(\pi/2)(X)$-pulse with phase ψ is the editing pulse. (*a*) Basic X-half-filter element. (*b*) X-half-filter element with spin-lock purge pulse (denoted SL). The spin-lock purge pulse has the same phase as the immediately preceding $(\pi/2)(^1H)$-pulse of the 2D [$^1H,^1H$]-NMR experimental scheme into which the half-filter element is inserted. Its duration is typically 1–2 ms. (*c*) X-half-filter element with refocusing delay. (*d*) 2-step phase cycle of the $\pi(^1H)$-pulse.

protons H. Therefore, if the delay τ is chosen to be $1/2^1J(^1H,X)$, the evolution under the scalar coupling Hamiltonian during this relatively short time period can be neglected for all coupling constants other than $^1J(^1H,X)$. If the X-bound protons are designated H and all other protons are I, then we have that in-phase proton magnetization $H_x + I_x$ evolves as follows:

$$H_x + I_x \xrightarrow{\tau/2 - \pi_\zeta(^1H) - \pi_x(X) - \tau/2} 2H_y X_z + I_x. \tag{6}$$

The following pair of $(\pi/2)(X)$-pulses (Fig. 14a) inverts the sign of the antiphase magnetization $2H_yX_z$ if the phase ψ of the editing pulse is x, but leaves the sign unaltered for $\psi = -x$. In either of the two cases the in-phase magnetization of the protons I is unaffected by the editing pulse:

$$2H_yX_z + I_x \xrightarrow{\ (\pi/2)_x(X)-(\pi/2)_{\pm x}(X)\ } \mp 2H_yX_z + I_x. \tag{7}$$

As a consequence, the difference between the data sets recorded with $\psi = x$ and $\psi = -x$ contains only the $2H_yX_z$ terms, which arise from the X-bound protons, whereas the sum of the two data sets contains the I_x terms, which come from all other hydrogens. The sum spectrum and the difference spectrum are 90° out of phase relative to each other.

Fig. 14b shows an extension of the basic X-half-filter element by a ^{1}H spin-lock purge pulse (Otting & Wüthrich, 1988). Due to the spatial inhomogeneity of the radio-frequency field, the spin-lock pulse efficiently defocuses all the components of the proton magnetization that are perpendicular to the spin-lock axis, while the magnetization parallel to the spin-lock axis is retained:

$$2H_yX_z + I_x \xrightarrow{\ SL_y(^1H)\ } 2H_yX_z. \tag{8}$$

The spin-lock purge pulse thus improves the selection for the resonances of X-bound protons in the subspectrum obtained as the difference of the data sets recorded with $\psi = x$ and $\psi = -x$. On the other hand, one looses the subspectrum obtained as the sum of the two data sets, which originates from the terms I_x. (The spin-lock can also be used to improve the observation of ^{13}C or ^{15}N satellites at natural abundance, when insufficient suppression of the main signals from the protons bound to ^{12}C or ^{14}N is obtained by the use of phase cycling only.)

Fig. 14c shows a X-half-filter with refocusing delay, which is based on the spin-echo difference experiment (Emshwiller *et al.* 1960). Starting from in-phase magnetization $H_x + I_x$ one obtains for $\tau = 1/2^1\mathcal{J}(^1H,X)$:

$$\left.\begin{aligned}
H_x &\xrightarrow{\ \tau\ } 2H_yX_z \xrightarrow{\ (\pi)_\zeta(^1H)-(\pi/2)_x(X)-(\pi/2)_{\pm x}(X)\ } \pm 2H_yX_z \xrightarrow{\ \tau\ } \mp H_x \\
I_x &\xrightarrow{\ \ } I_x \qquad\qquad\qquad\qquad\qquad\qquad\ \longrightarrow I_x \qquad \longrightarrow I_x.
\end{aligned}\right\} \tag{9}$$

In writing equation (9) the evolution under the chemical shift Hamiltonian was neglected, since the $\pi(^1H)$-pulse in the middle of the filter delay 2τ refocuses the chemical shift evolution. As a consequence only the evolution under scalar coupling is relevant. Refocusing of the heteronuclear antiphase magnetization offers the possibility of decoupling the proton signals with a heteronuclear broadband decoupling sequence after the X-half-filter. This scheme also has the advantage of achieving the editing effect with fewer pulses than the alternative schemes of Fig. 14(a, b), and is therefore less prone to deterioration of the resulting spectrum due to pulse imperfections.

A complete description of the X-half-filter must also include scalar proton–proton couplings and small two-bond and longer-range heteronuclear couplings. We first analyse the effects from homonuclear proton–proton couplings in a
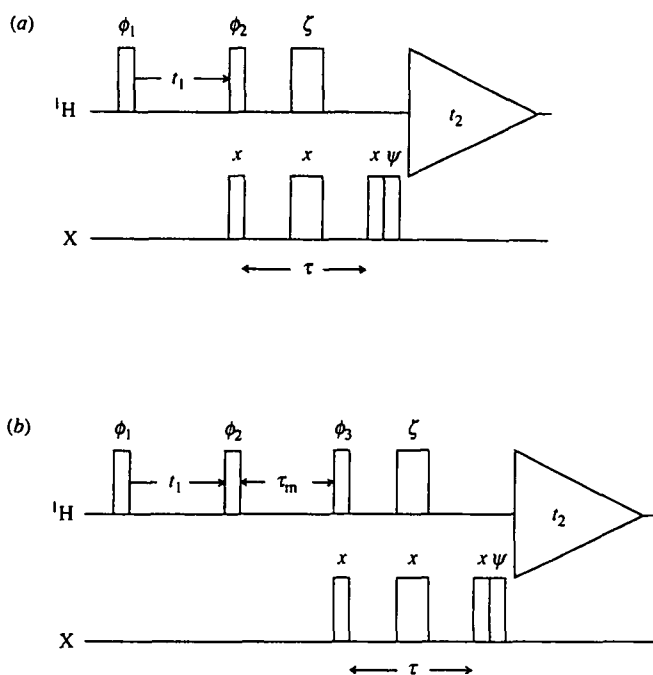
system containing a X-bound proton H which is coupled to another proton spin I by the coupling constant $\mathcal{J}_{HI}$, and two protons I and I′ which are coupled to each other by the coupling constant $\mathcal{J}_{II'}$. Starting from in-phase magnetization H_x and I_x, antiphase magnetization is generated during the filter delay $2\tau = 1/2\,^1\mathcal{J}(^1H,X)$ of the X half-filter element with refocusing (Fig. 14c):

$$
\begin{aligned}
H_x &\xrightarrow{\tau-(\pi)_\zeta(^1H)-(\pi/2)_x(X)-(\pi/2)_{\pm x}(X)-\tau} \mp\cos\pi\mathcal{J}_{HI}2\tau\,H_x \mp \sin\pi\mathcal{J}_{HI}2\tau\,2H_y\,I_z \\
I_x &\xrightarrow{\hspace{4.5cm}} \cos\pi\mathcal{J}_{II'}\,2\tau\,I_x + \sin\pi\mathcal{J}_{II'}\,2\tau\,2I_y\,I'_z.
\end{aligned}
\right\} \qquad (10)
$$

For a short delay $\tau = 1/2\mathcal{J}_{HX} = 1/2\,^1\mathcal{J}(^1H,X)$, the terms $2H_yI_z$ and $2I_yI'_z$ lead to minor multiplet distortions of the in-phase signals represented by H_x and I_x, respectively [equation (9)]. Because of the large linewidths the effect is hardly visible in the ^{1}H-NMR spectra of macromolecules, and it is further reduced with the X-half-filter elements of Fig. 14(a, b), where less antiphase magnetization is generated because of the shorter filter delay.

The presence of small heteronuclear coupling constants $\mathcal{J}_{HX}$ does not lead to a phase distortion of the multiplet fine structure. However, the editing procedure of a X-half-filter tuned to the big one-bond coupling constant $^1\mathcal{J}(^1H,X)$ distributes the intensity of resonances with small heteronuclear couplings unequally between the sum spectrum and the difference spectrum (Table 3). This *cross-talk* is further discussed in section 7.

All three X-half-filter elements of Fig. 14(a–c), can be used with a wide variety of ^{1}H-NMR experiments. Initially, mainly for technical reasons, the elements of Fig. 14(a, b), were applied, which do not allow heteronuclear decoupling during the detection period (Otting *et al.* 1986). These schemes are still useful for special purposes, for example, for measurements of small heteronuclear coupling constants in the simplified subspectra obtained by editing with $^1\mathcal{J}(^1H,X)$. For such studies the experiments of Fig. 14(a, b), have the additional advantage that distortions of the multiplet fine structures due to homonuclear antiphase coherence are minimized. Conversely, considering the 2-fold increase of the effective sensitivity for observation of the desired signals (assuming that relaxation during the prolonged filter delay can be neglected) and the additional simplification of the subspectra that result from heteronuclear broadband decoupling, the half-filter element with refocusing delay (Fig. 14c) will foreseeably be most widely used in the future.

5.2 *X-half-filters in [$^1H,^1H$]-COSY and [$^1H,^1H$]-NOESY*

5.2.1 *[$^1H,^1H$]-COSY and [$^1H,^1H$]-NOESY with $X(\omega_2)$-half-filter*

Fig. 15 shows the experimental schemes obtained by addition of the X-half-filter element of Fig. 14a to the [^{1}H,^{1}H]-COSY and [^{1}H,^{1}H]-NOESY pulse schemes of Figs 10a and 11a. The phase cycling priority list for [^{1}H,^{1}H]-COSY is: ψ, 2-step-CYCLOPS, ϕ_2, ζ, ϕ_1, and repetition with permuted order of ψ, which results in a 64-step phase cycle. The receiver phase changes whenever the phase of ϕ_1 is changed (see Fig. 10b). For [^{1}H,^{1}H]-NOESY with $X(\omega_2)$-half-filter the phase cycling priority is: ψ, 2-step-CYCLOPS, ϕ_3, ϕ_2, ζ, ϕ_1, and repetition with

Fig. 15. Experimental schemes with X(ω_2)-half-filter. (a) [^{1}H,^{1}H]-COSY. (b) [^{1}H,^{1}H]-NOESY. The phase cycles are described in the text.

permuted order of ψ, which leads to a 128-step phase cycle. The receiver phase changes with ϕ_1, ϕ_2 and ϕ_3 (see Fig. 11 b).

In a product operator calculation starting from equilibrium magnetization of the X-bound protons, H_z, and the other protons, I_z, one finds the following coherences at the start of the detection period:

$$\underset{H_z \xrightarrow{\hspace{3cm}}}{\overset{\text{[^{1}H,^{1}H]-COSY with (ω_2)-half-filter}}{}} \mp \sin \Omega t_1 \cos \pi \mathcal{J}_{HX} t_1\, 2H_y X_z \left.\begin{array}{c} \\ \\ \end{array}\right\} \qquad (11)$$
$$I_z \xrightarrow{\hspace{3cm}} \sin \Omega t_1\, I_x.$$

$$\underset{H_z \xrightarrow{\hspace{3cm}}}{\overset{\text{[^{1}H-^{1}H]-NOESY with X(ω_2)-half-filter}}{}} \mp \cos \Omega t_1 \cos \pi \mathcal{J}_{HX} t_1\, 2H_x X_z \left.\begin{array}{c} \\ \\ \end{array}\right\} \qquad (12)$$
$$I_z \xrightarrow{\hspace{3cm}} -\cos \Omega t_1\, I_y.$$

In equations (11) and (12) the delay τ is assumed to be $1/2\mathcal{J}_{HX} = 1/2^1\mathcal{J}(^1\text{H},\text{X})$. The upper and lower signs correspond to the different signs of the phase ψ of the editing pulse. The heteronuclear antiphase magnetizations $H_y X_z$ and $H_x X_z$ contribute to the difference spectra, and the in-phase terms I_x and I_y lead to peaks in the sum spectra. It is seen that the sum and the difference spectra are of the same phase in ω_1 (for both the trigonometric dependence on t_1 is either symmetric or antisymmetric with respect to $t_1 = 0$), but in the ω_2 dimension the spectra are 90° out of phase relative to each other, as is evidenced by the product operators $H_y X_z$ and I_x in equation (11), and $H_x X_z$ and I_y in equation (12), respectively. The difference spectrum is in-phase along ω_1 with respect to the heteronuclear coupling $\mathcal{J}_{HX}$, and antiphase along ω_2. Thus the spectra can be decoupled along ω_1

either by broadband irradiation at the frequency of X or with the use of a $\pi(X)$-pulse in the middle of the t_1 period, but no heteronuclear decoupling may be used during the detection period. If no decoupling is used during the evolution time t_1, a $(\pi/2)(X)$-pulse should be applied immediately before the $X(\omega_2)$-half-filter delay (Fig. 15) in order to convert any heteronuclear antiphase magnetization present at the end of the evolution time into unobservable multiple-quantum coherence. Otherwise the heteronuclear antiphase magnetization would refocus to in-phase magnetization during the delay τ. As in-phase magnetization is insensitive to the editing pulse, it would then appear in the sum spectrum although it comes from X-bound protons (Otting et al. 1986).

5.2.2 Experimental examples

Fig. 16 shows the spectral region ($\omega_1 = 6\cdot6$–$9\cdot3$ ppm, $\omega_2 = 6\cdot6$–$9\cdot3$ ppm) from the same difference spectrum of NOESY with $^{15}N(\omega_2)$-half-filter as in Fig. 8, which was recorded with a preparation of the N-terminal domain 1–76 of Salmonella phage P22 c2 repressor that had all 10 Leu residues labelled with ^{15}N (Fig. 6). This region contains the diagonal peaks of the amide protons of all 10 Leu residues, and cross-peaks between pairs of ^{15}N-labelled amide protons of Leu as well as between amide protons of Leu and unlabelled amide protons. The diagonal peaks of the ^{15}N-bound protons are split into four components by the one-bond ^{15}N–^1H scalar coupling of ca. 90 Hz (Fig. 16a). Nuclear Overhauser effects between different ^{15}N-bound protons give rise to pairs of cross-peaks symmetrically arranged with respect to the diagonal, which are split into four components by one-bond ^{15}N–^1H scalar couplings along both ω_1 and ω_2 (Fig. 16a). The NOESY cross-peaks representing NOEs between leucine amide protons and protons not bound to ^{15}N consist of two fine structure components separated by the ^{15}N–^1H scalar coupling along ω_2, and they are observed only once, either above or below the diagonal. The cross peaks identified in Fig. 16b are between ^{15}N–^1H and ^{14}N–^1H and those in Fig. 8 between ^{15}N–^1H and $^{12}C^\alpha$–^1H. All the peak identifications indicated in Figures 8 and 16 were quite easy to obtain in the well resolved difference spectra (Senn et al. 1987; see Fig. 1b for a comparison with a complete, unfiltered [^1H,^1H]-NOESY spectrum). A special advantage, in this particular instance, of working with an undecoupled spectrum with X-half-filter is seen in the region near ($\omega_1 = 7\cdot05$, $\omega_2 = 7\cdot05$ ppm): Although aromatic ring protons of Tyr63 and the amide proton of Leu64 have virtually identical chemical shifts the cross-peak between these two resonances could be resolved, because the diagonal peak of Leu 64 ^{15}N–^1H is split along ω_1 by the $^1\mathcal{J}(^1H,^{15}N)$ coupling constant, whereas the cross-peak with Tyr63 is not split along ω_1 (Fig. 16a).

5.2.3 [^1H,^1H]-COSY and [^1H,^1H]-NOESY with $X(\omega_2)$-half-filter and heteronuclear decoupling

Fig. 17 shows the experimental schemes of [^1H,^1H]-COSY and [^1H,^1H]-NOESY with $X(\omega_2)$-half-filter and heteronuclear decoupling. Decoupling is achieved in ω_1 with a refocusing $\pi(X)$-pulse during the evolution period, and in ω_2 by heteronuclear broadband decoupling during the detection period. These
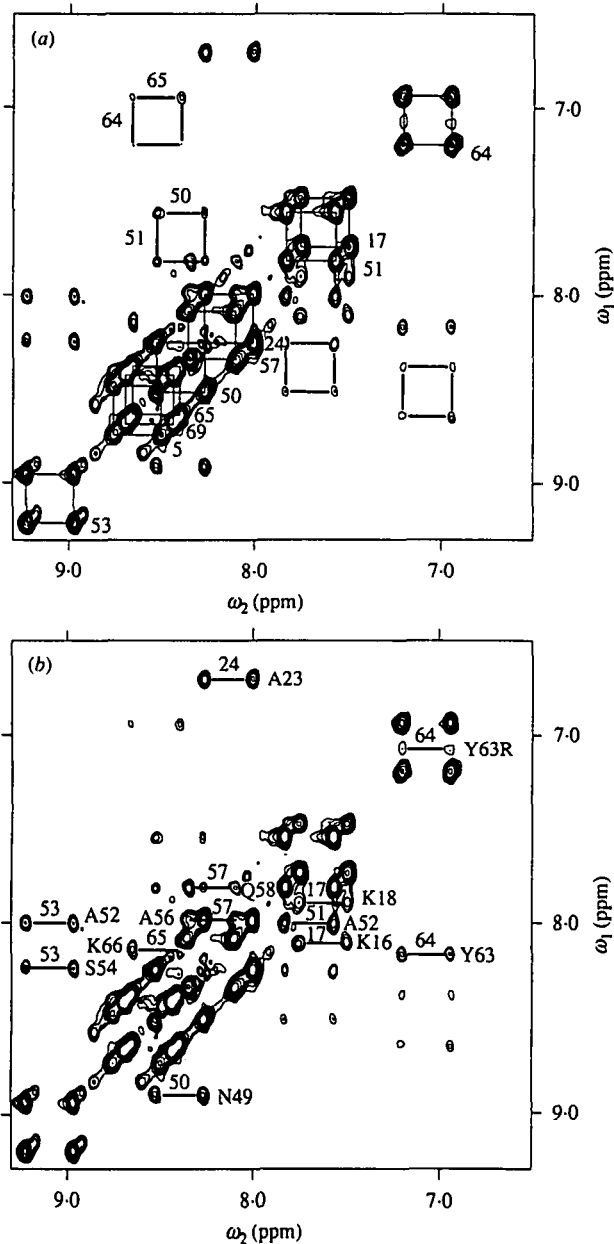
Fig. 16. Spectral region ($\omega_1 = 6\cdot6$–$9\cdot3$ ppm, $\omega_2 = 6\cdot6$–$9\cdot3$ ppm) of the same difference spectrum from [^{1}H,^{1}H]-NOESY with ^{15}N(ω_2)-half-filter as in Fig. 8. The experiment was recorded with the pulse sequence of Fig. 15b with a solution of P22 c2 repressor 1–76 in which all 10 Leu residues were labelled with ^{15}N. The multiplets are in-phase along ω_1 and antiphase along ω_2. Positive and negative levels are plotted without distinction. In (a) the fine structure components of 10 diagonal peaks from [2–^{15}N]-Leu are connected by thin lines, and cross-peaks between two ^{15}N-bound amide protons of different leucyl residues are identified by thicker lines. The peaks are identified with the sequence numbers of the corresponding Leu residues. In (b) the fine structure components of cross-peaks between labelled amide protons of Leu and unlabelled amide protons are connected by horizontal lines and identified with the Leu sequence number and the one-letter symbol and the sequence position of the second residue. (From Senn *et al.* 1987a.)
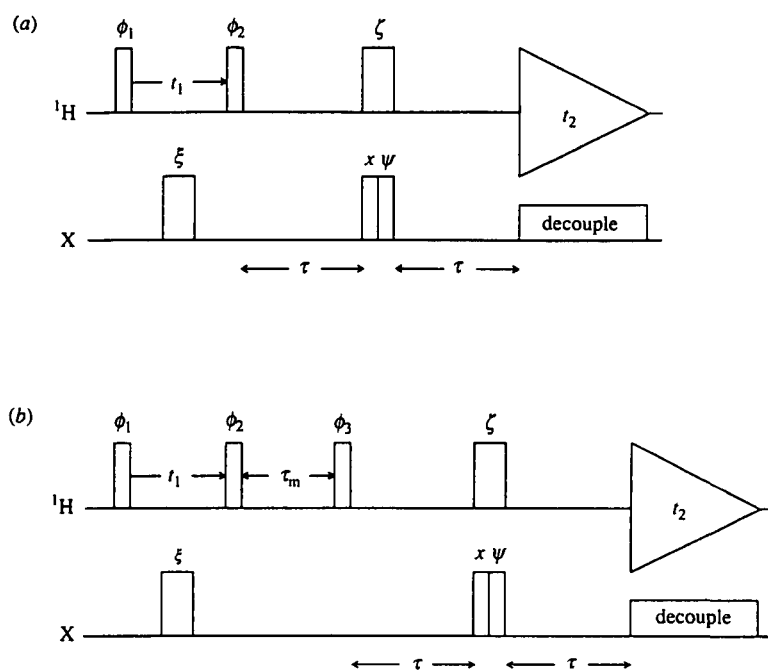
Fig. 17. Experimental schemes with $X(\omega_2)$-half-filter and heteronuclear broadband decoupling. (a) [^{1}H,^{1}H]-COSY. (b) [^{1}H,^{1}H]-NOESY. The phase cycles are described in the text.

experimental schemes use the half-filter element of Fig. 14c. To eliminate artefacts from imperfections of the $\pi(X)$-pulse, the phase ξ should be alternated between x and $-x$ independently of the rest of the phase cycle. The receiver phase stays constant when the phases ξ and ζ of the π-pulses are alternated. We recommend the following phase cycling priority list for the COSY experiment: ψ, 2-step CYCLOPS, ϕ_2, ζ, ξ, ϕ_1, and repetition with permuted order of ψ, resulting in a 128-step phase cycle. The corresponding phase cycling priority list for the NOESY experiment is: ψ, 2-step CYCLOPS, ϕ_3, ϕ_2, ζ, ξ, ϕ_1, and repetition with permuted order of ψ, which leads to a 256-step phase cycle. The phase cycle can be shortened if the $(\pi)_\xi(X)$-pulse in the middle of t_1 is replaced by heteronuclear broadband irradiation. The editing rules for obtaining the sum spectrum and the difference spectrum are the same as for the corresponding experiments without refocusing and heteronuclear decoupling. The product operator description for the experiments with heteronuclear decoupling in equations (13) and (14) is largely analogous to equations (11) and (12):

[^{1}H,^{1}H]-COSY with $X(\omega_2)$-half-filter and refocusing

$$
\left.
\begin{aligned}
H_z &\xrightarrow{\hspace{4cm}} \mp \sin \Omega t_1 \, H_x \\
I_z &\xrightarrow{\hspace{4cm}} \sin \Omega t_1 \, I_x .
\end{aligned}
\right\} \qquad (13)
$$

[^{1}H,^{1}H]-NOESY with $X(\omega_2)$-half-filter and refocusing

$$
\left.
\begin{aligned}
H_z &\xrightarrow{\hspace{4cm}} \pm \cos \Omega t_1 \, H_y \\
I_z &\xrightarrow{\hspace{4cm}} - \cos \Omega t_1 \, I_y .
\end{aligned}
\right\} \qquad (14)
$$

The delay τ is again assumed to be $1/2^1\!\mathcal{J}(^1\text{H},\text{X})$, and the upper and lower signs reflect the sign of the editing pulse. It is seen from equations (13) and (14) that the sum and the difference spectrum have the same phase in both dimensions.

5.2.4 *Experimental examples*

Experiments using [^{1}H,^{1}H]-NOESY with ^{15}N(ω_2)-half-filter and heteronuclear decoupling (Fig. 17b) were first used by Fesik *et al.* (1987) in a study of a polypeptide with the sequence of residues 7–23 from atrial natriuretic factor. In this synthetic polypeptide the residues Gly10, Ala17 and Gly20 were labelled with ^{15}N, and the peptide was bound to perdeuterated SDS micelles. This study presents a nice illustration of both, the simplification of the X-half-filter difference spectrum, and the fact that the sum spectrum is devoid of cross-peaks with labelled protons (Table 1). Fig. 18 compares the conventional [^{1}H,^{1}H]-NOESY spectrum (Fig. 18a) with the difference spectrum (Fig. 18b) and the sum spectrum (Fig. 18c) obtained from [^{1}H,^{1}H]-NOESY with ^{15}N(ω_2)-half-filter. The spectral region shown contains the diagonal peaks of the amide protons, and the cross peaks between the amide protons along ω_2 and all other proton types along ω_1. The difference spectrum (Fig. 18b) selects the amide proton resonances of the three ^{15}N-labelled amino-acid residues in the ω_2 dimension, while these resonances are suppressed in the sum spectrum. The difficulties in the spectral interpretation that arose because of the overlap between the pairs of amide proton resonances of residues 18 and 20, 10 and 11, and 17 and 21 (Fig. 18a) were unambiguously resolved with the availability of the spectra of Fig. 18(b, c). The phase cycle used by Fesik *et al.* (1987) did not include the phase alternation of the $(\pi)_\zeta(^1\text{H})$-pulse of the ^{15}N-half-filter element. This leads to phase distortions along ω_2, which become noticeable in the intense diagonal peaks of Fig. 18c.

[^{1}H,^{1}H]-NOESY experiments recorded with a ^{15}N(ω_2)-half-filter and decoupling were also used to study the conformation of the inhibitor peptide and to identify the inhibitor-enzyme contacts in a complex of a ^{15}N-labelled tripeptide inhibitor with pepsin (Fesik, 1988; Fesik *et al.* 1988). Fig. 19 shows the difference spectra from [^{1}H,^{1}H]-NOESY with ^{15}N(ω_2)-half-filter of three different preparations obtained with differently ^{15}N-labelled peptide inhibitors. The spectral region shown contains the diagonal peaks of the ^{15}N-bound amide protons, and cross-peaks with these amide protons. (A conventional [^{1}H,^{1}H]-NOESY spectrum would contain over 1000 peaks in the same spectral region.) The cross-peaks observed in the difference spectra represent either intramolecular NOEs within the inhibitor peptide, or intermolecular NOEs between the amide protons of the peptide and protons of the enzyme. The assignment of the intramolecular NOEs was obtained from spectral comparisons of complexes containing differently deuterated peptide inhibitors (Fig. 19). Intermolecular NOEs between inhibitor and enzyme were observed in the corresponding complexes with ^{13}C-labelled inhibitors using [^{1}H,^{1}H]-NOESY with ^{13}C(ω_2)-half-filter and decoupling. The resonances of the ^{13}C-bound protons of the inhibitor could be assigned from a [^{13}C,^{1}H]-COSY spectrum (Bax *et al.* 1983) of the
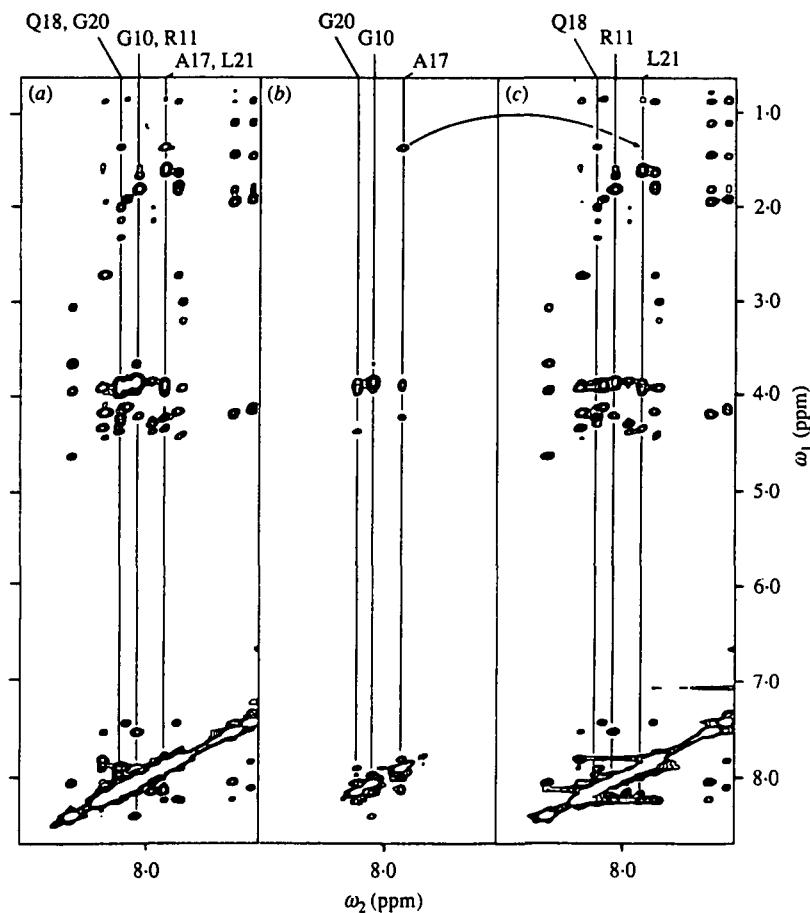
Fig. 18. 2D [^{1}H,^{1}H]-NMR spectra of the fragment 7–23 from the atrial natriuretic factor, CFGGRIDRIGAQSGLGC. The residues G10, A17 and G20 were labelled with ^{15}N, and the peptide was studied in SDS micelles (peptide concentration 10 mM in H$_2$O, 200 mM perdeuterated sodium-dodecylsulphate, $T = 40$ °C, proton frequency 500 MHz). The data were multiplied with a cosine window function in both dimensions before Fourier transformation, and a baseline correction was applied. (*a*) Conventional [^{1}H,^{1}H]-NOESY spectrum acquired with a mixing time of 200 ms and ^{15}N-decoupling in ω_1 and ω_2. (*b*) Difference spectrum from [^{1}H,^{1}H]-NOESY recorded with a X(ω_2)-half-filter with refocusing and ^{15}N-decoupling in ω_1 and ω_2. The spectrum was recorded with the experimental scheme of Fig. 17*b*, with $\tau = 5.38$ ms. (*c*) Sum spectrum from the same data set as (*b*). Note that the NOEs involving the ^{15}N-labelled amide protons are absent from the sum spectrum (Table 1). As a specific example, the arrow from (*b*) into (*c*) connects the intraresidual cross peak between the amide proton and the methyl group of A17 in spectrum (*b*) with the corresponding empty area in (*c*). At the top the amide proton chemical shifts for G10, R11, A17, Q18, G20 and L21 are identified along ω_2. (From Fesik *et al.* 1987.)

complex. The assigned intramolecular ^{1}H–^{1}H NOEs of the peptide contain the desired information for elucidating the conformation of the peptide inhibitor in the complex (Fesik *et al.* 1988). For an identification of the contact sites in the enzyme, additional labelling experiments may be needed.
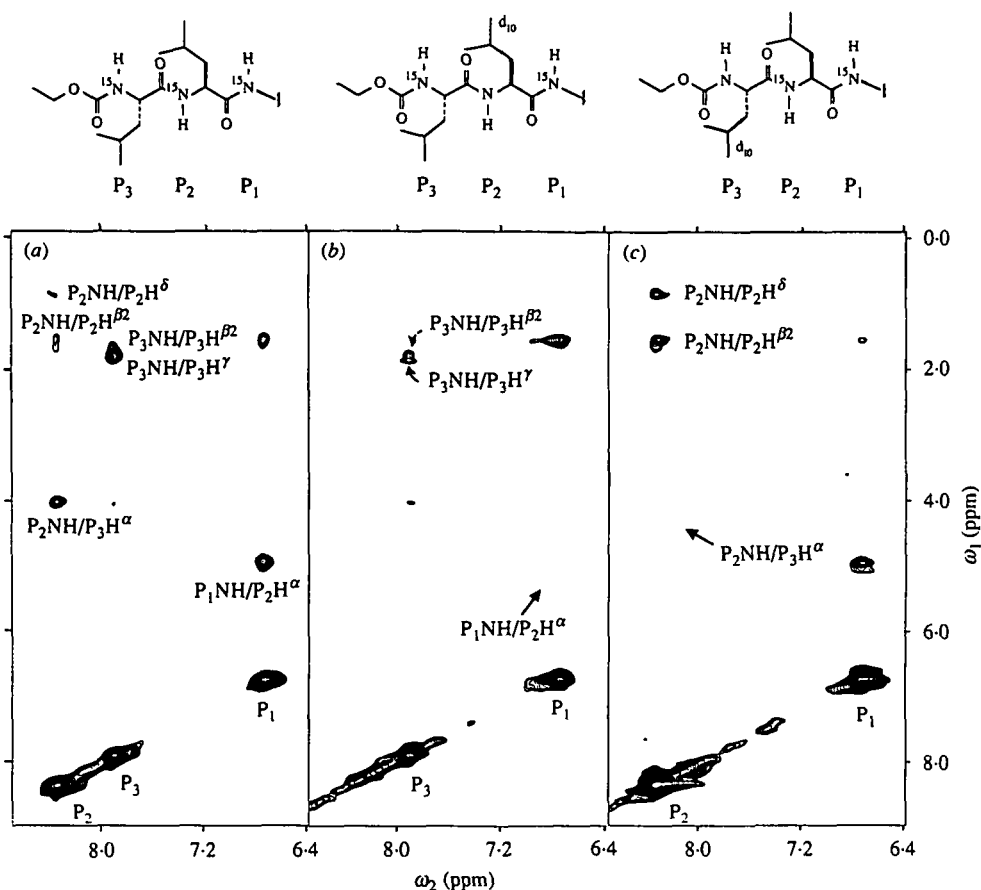
Fig. 19. Difference spectra from [^{1}H,^{1}H]-NOESY with ^{15}N(ω_2)-half-filter and ^{15}N-decoupling of three pepsin complexes with differently ^{15}N-labelled and partially deuterated inhibitors. (Concentration of the complex 1 mM in H_2O, pH 3·7, total measuring time about 54 h, mixing time 50 ms, $t_{1\,max} = 14·1$ ms, proton frequency 500 MHz, the experimental scheme of Fig. 17b was used.) Before Fourier transformation the data were exponentially multiplied in both dimensions, resulting in a linebroadening of 30 Hz. Part of the structure of the inhibitor peptide is shown at the top of the three spectra. (*a*) All three amino-acid residues P_1 to P_3 of the inhibitor were labelled with ^{15}N. The diagonal peaks of the three amide protons are indicated by P_1, P_2 and P_3, and assignments are also given for the cross-peaks representing intraresidual and sequential NOEs within the peptide. (*b*) The amino-acid residues P_1 and P_3 were labelled with ^{15}N and the side chain of P_2 was deuterated. (*c*) The amino-acid residues P_1 and P_2 were labelled with ^{15}N and the side chain of P_3 was deuterated. In (*b*) and (*c*), straight arrows indicte locations in the spectra where sequential cross-peaks are absent due to the deuterium labelling. (From Fesik *et al.* 1988).

Torchia *et al.* (1989) assigned virtually all backbone proton resonances of staphylococcal nuclease in a ternary complex with Ca^{2+} and thymidine-3′,5′-diphosphate. Thereby [^{1}H,^{1}H]-NOESY with ^{15}N(ω_2)-half-filter and decoupling was one of the key experiments for identifying the sequential NOE connectivities in protein preparations with residue-selective ^{15}N labelling. For this project more
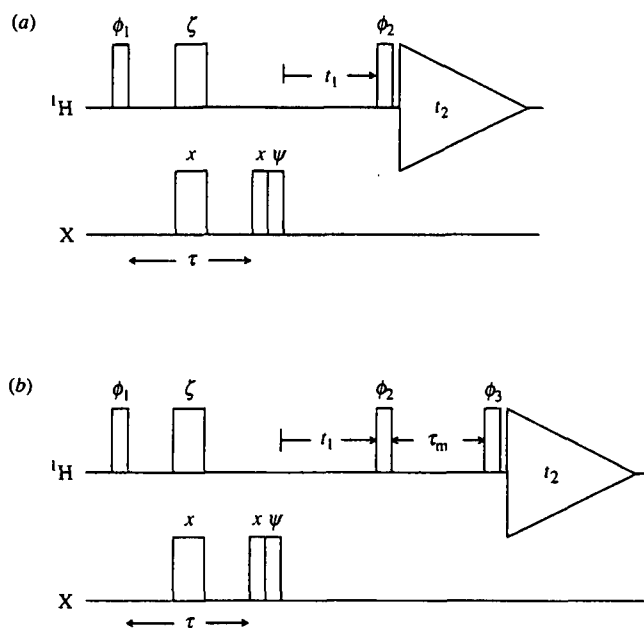
Fig. 20. Experimental schemes with $X(\omega_1)$-half-filter. (a) [^{1}H,^{1}H]-COSY. (b) [^{1}H,^{1}H]-NOESY. The phase cycles are described in the text.

than 20 different protein preparations were used, which contained ^{15}N and/or ^{13}C labels in one or several amino-acid types.

Fesik *et al.* (1989) used the experiment of Fig. 17b to record a [^{1}H,^{1}H]-NOESY spectrum with ^{15}N(ω_2)-half-filter of a uniformly ^{15}N-labelled protein–inhibitor complex of molecular weight 27 500, and demonstrated for this uniformly enriched sample that significantly improved spectral resolution could be obtained with the corresponding heteronuclear 3D NMR experiment (see Fig. 9).

5.2.5 [^{1}H,^{1}H]-COSY and [^{1}H,^{1}H]-NOESY with $X(\omega_1)$-half-filter

Fig. 20 shows the experimental schemes for [^{1}H,^{1}H]-COSY and [^{1}H,^{1}H]-NOESY with $X(\omega_1)$-half-filter. In these schemes the X-half-filter element of Fig. 14a was inserted between the excitation pulse and the evolution time t_1 of the standard [^{1}H,^{1}H]-COSY and [^{1}H,^{1}H]-NOESY experiments (Figs 10, 11). The phase cycling is the same as for the corresponding experiments with $X(\omega_2)$-half-filter (Fig. 15). The $X(\omega_1)$-half-filter is active only before the evolution period and therefore affects only the ω_1 frequency domain. In full analogy to the $X(\omega_2)$-half-filter technique the two data sets recorded with different phases ψ of the editing $(\pi/2)(X)$-pulse are added or subtracted to yield a sum spectrum and a difference spectrum (Tables 1 and 3). Along the ω_1 frequency axis, the sum spectrum contains all the resonances from the protons which are not bound to X, and the difference spectrum contains only resonances from X-bound protons. A product

operator calculation analogous to equations (11) and (12) shows that the following terms are generated at the start of the detection period t_2:

[^{1}H,^{1}H]-COSY with X(ω_1)-half-filter

$$H_z \xrightarrow{\hspace{4cm}} \left. \begin{array}{l} \pm \cos \Omega t_1 \cos \pi \mathcal{J}_{HX} t_1 \, 2H_z X_z \\ \mp \sin \Omega t_1 \sin \pi \mathcal{J}_{HX} t_1 \, H_x \end{array} \right\}$$

$$I_z \xrightarrow{\hspace{4cm}} -\sin \Omega t_1 \, I_x . \qquad \left. \right\} \tag{15}$$

[^{1}H,^{1}H]-NOESY with X(ω_1)-half-filter

$$H_z \xrightarrow{\hspace{4cm}} \left. \begin{array}{l} \mp \sin \Omega t_1 \cos \pi \mathcal{J}_{HX} t_1 \, 2H_y X_z \\ \mp \cos \Omega t_1 \sin \pi \mathcal{J}_{HX} t_1 \, H_y \end{array} \right\}$$

$$I_z \xrightarrow{\hspace{4cm}} -\cos \Omega t_1 \, I_y . \qquad \left. \right\} \tag{16}$$

In this calculation the delay τ has been assumed to be $1/2\mathcal{J}_{HX} = 1/2{}^1\mathcal{J}(^1H,X)$, and the upper and lower signs correspond to the presence or absence of the effective $\pi(X)$-editing pulse. The first two terms of equations (15) and (16) contribute to the difference spectra. Their multiplet fine structures are complementary in the sense that one term is antiphase with respect to $\mathcal{J}_{HX}$ and the other is in-phase. As a result, half of the multiplet components are cancelled out and an E. COSY-type multiplet pattern (Griesinger *et al.* 1986) is observed both for the diagonal peaks and the cross-peaks (Wörgötter *et al.* 1988; Montelione *et al.* 1989). This unique fine structure makes experiments with X(ω_1)-half-filters attractive for measurements of small heteronuclear multiple-bond coupling constants, which are usually not resolved in the ^{1}H-NMR spectra of macromolecules. The conventional multiplet patterns can be restored by insertion of a $(\pi/2)_x(X)$-pulse during the mixing period, similar to Fig. 15. This pulse converts the heteronuclear antiphase magnetization of equations (15) and (16) into unobservable two-spin coherence, so that only the second term can be detected.

As was mentioned earlier, E. COSY-type multiplet patterns for X-coupled protons are observed quite generally in conventional 2D [^{1}H,^{1}H]-NMR spectra of molecules labelled with, for example, ^{13}C, ^{15}N or ^{113}Cd. Nonetheless the X(ω_1)-half-filter stands out as a powerful technique for selecting the signals from X-bound protons and for measurements of small heteronuclear coupling constants. The selection for X-bound protons is particularly clean with the use of the filter element of Fig. 14*b*, which suppresses the magnetization from the unlabelled protons with a spin-lock purge pulse. In this version the experiment is also suitable for studies of compounds with natural abundance of ^{13}C and ^{15}N (Otting & Wüthrich, 1988).

5.2.6 *Experimental examples*

The first 2D [^{1}H,^{1}H]-NMR experiment with a heteronuclear filter was performed by Bolton (1985) with ^{13}C-labelled glucose. He applied a heteronuclear zero-quantum filter, which differs from the X-half-filter-element of Fig. 14*a* by the fact that a 4-step phase cycle was used for the phase ψ of the $(\pi/2)(X)$-editing pulse. The [^{1}H,^{1}H]-COSY spectrum thus obtained had E. COSY-type multiplet patterns as predicted from equation (15). The experiment was subsequently

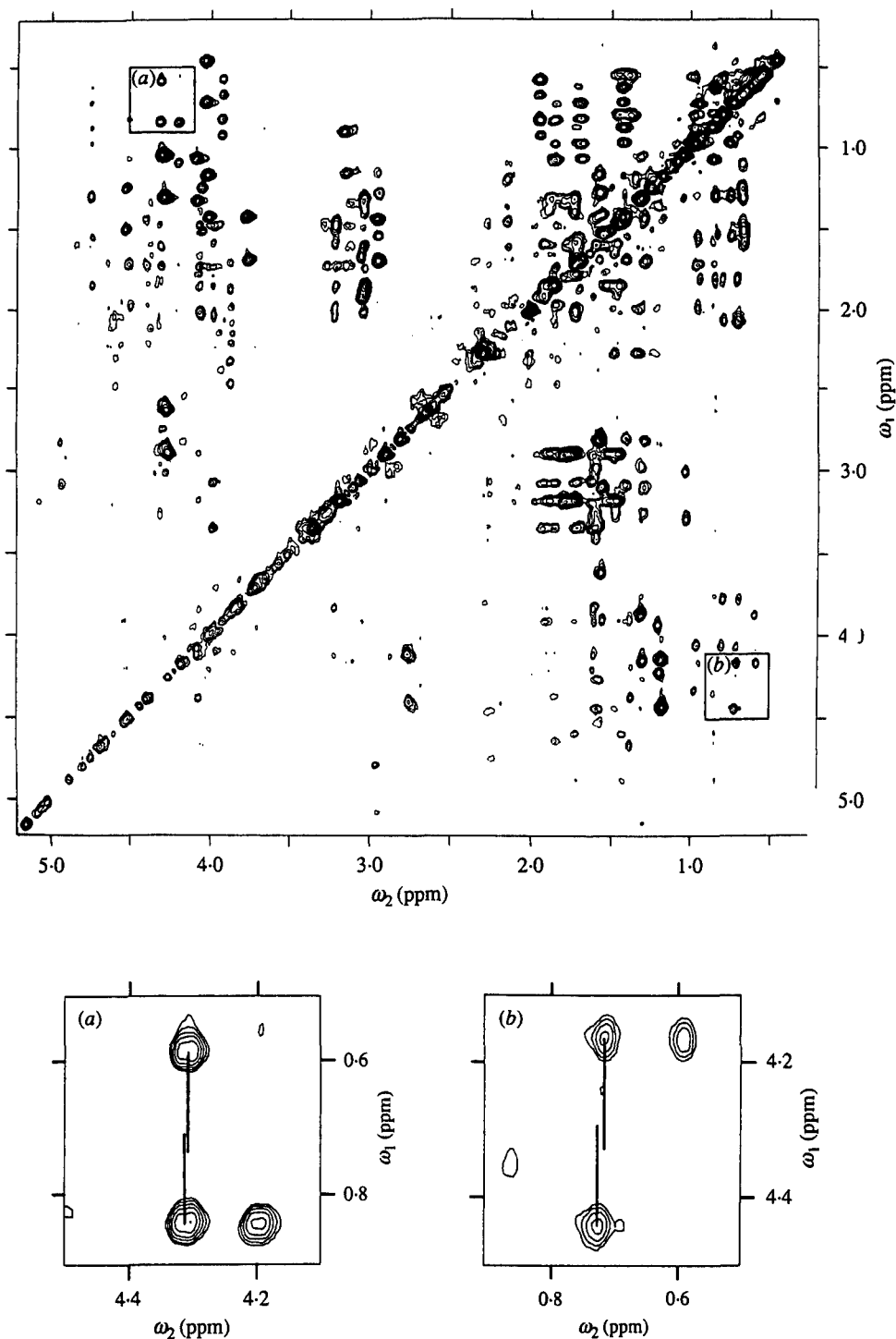Fig. 21. [^{1}H,^{1}H]-TOCSY spectrum of the unlabelled protein basic pancreatic trypsin inhibitor (BPTI) recorded with a ^{13}C(ω_1)-half-filter. (Protein concentration 20 mM in D_2O, pD 4·6, 36 °C, mixing time 60 ms, $\tau = 3\cdot4$ ms, ^{1}H frequency 500 MHz, total recording time about 33 h.) The pulse scheme used was derived from the experimental scheme of Fig. 20 *a*

modified so as to enable heteronuclear decoupling in both dimensions, and was applied to staphylococcal nuclease labelled with ^{13}C in the 3,5-positions of tyrosine (Wilde *et al.* 1986). Overall the heteronuclear zero-quantum filter leads to similar results as the filter elements of Fig. 14, except for a 2-fold reduction of the signal-to-noise ratio. The zero-quantum filter-element is therefore not further treated here.

As an illustration of the use of the filter element with spin-lock purge pulse (Fig. 14*b*), Fig. 21 shows a [^{1}H,^{1}H]-TOCSY spectrum of unlabelled basic pancreatic trypsin inhibitor (BPTI) recorded with a ^{13}C(ω_1)-half-filter and a spin-lock purge pulse at the end of the filter delay to select the ^{13}C-satellites at natural abundance. The phase cycling is the same as for the [^{1}H,^{1}H]-COSY experiment with X(ω_1)-half-filter. In Fig. 21 the expansions (*a*) and (*b*) show the ^{13}C$^\gamma \underline{H}_3$–C$^\alpha \underline{H}$ cross-peak of Ile19 and the corresponding ^{13}C$^\alpha \underline{H}$–C$^\gamma \underline{H}_3$ cross-peak on the opposite side of the diagonal. The multiplet components are separated along ω_1 by the one-bond coupling constant $^1\mathcal{J}(^1$H,^{13}C), and along ω_2 by the heteronuclear coupling constants $^3\mathcal{J}(C^\alpha \underline{H},^{13}\underline{C}^\gamma H_3)$ and $^3\mathcal{J}(C^\gamma \underline{H}_3,^{13}\underline{C}^\alpha H)$, respectively. The coupling constants measured from the relative displacement of the two multiplet components shown in the expansions (*a*) and (*b*) of Fig. 21 are $^3\mathcal{J}(C^\alpha \underline{H}-^{13}\underline{C}^\gamma H_3) = 2 \cdot 5$ Hz and $^3\mathcal{J}(C^\gamma \underline{H}_3-^{13}\underline{C}^\alpha H) = 5 \cdot 0$ Hz, respectively. The experiment thus provides easy access to accurate measurements of heteronuclear coupling constants that are smaller than the width of the ^{1}H NMR lines (Montelione *et al.* 1989).

5.2.7 [^{1}H,^{1}H]-COSY and [^{1}H,^{1}H]-NOESY with X(ω_1)-half-filter and heteronuclear decoupling

Fig. 22 shows the experimental schemes for [^{1}H,^{1}H]-COSY and [^{1}H,^{1}H]-NOESY combined with the X(ω_1)-half-filter element of Fig. 14*c*. The phase cycling is the same as for the corresponding experiments with X(ω_2)-half-filter. A product operator description analogous *to* equations (11) and (12) leads to the following coherences at the start of the detection period t_2:

[^{1}H,^{1}H]-COSY with X(ω_1)-half-filter and refocusing

$$\left. \begin{array}{l} H_z \xrightarrow{\hspace{6cm}} \pm \sin \Omega t_1 \, H_x \\ I_z \xrightarrow{\hspace{6cm}} - \sin \Omega t_1 \, I_x. \end{array} \right\} \tag{17}$$

by substituting the second $(\pi/2)(^1$H) pulse by the MLEV-17 mixing scheme of the clean-TOCSY experiment (Griesinger *et al.* 1988). The same phase cycle was used as in [^{1}H,^{1}H]-COSY with X(ω_1)-half-filter. A spin-lock purge pulse of 2 ms duration was used at the end of the filter delay (Fig. 14*b*) to improve the suppression of the signals from ^{12}C-bound protons in the difference spectrum. Along ω_1 the cross-peaks are split into two antiphase components by $^1\mathcal{J}(^1$H,^{13}C). Positive and negative levels are plotted without distinction. Two regions containing the cross-peak multiplets ^{13}C$^\gamma \underline{H}_3$–C$^\alpha \underline{H}$ (*a*) and ^{13}C$^\alpha \underline{H}$–C$^\gamma \underline{H}_3$ (*b*) of Ile19 are framed and displayed separately on an enlarged scale. In the expanded plots the vertical lines indicate the chemical shift positions along ω_2 of the fine structure components that belong to the same cross-peak. The separation between the two lines corresponds to the following long-range heteronuclear coupling constants: (*a*) $^3\mathcal{J}(C^\alpha \underline{H},^{13}\underline{C}^\gamma H_3)$, (*b*) $^3\mathcal{J}(C^\gamma \underline{H}_3,^{13}\underline{C}^\alpha H)$.
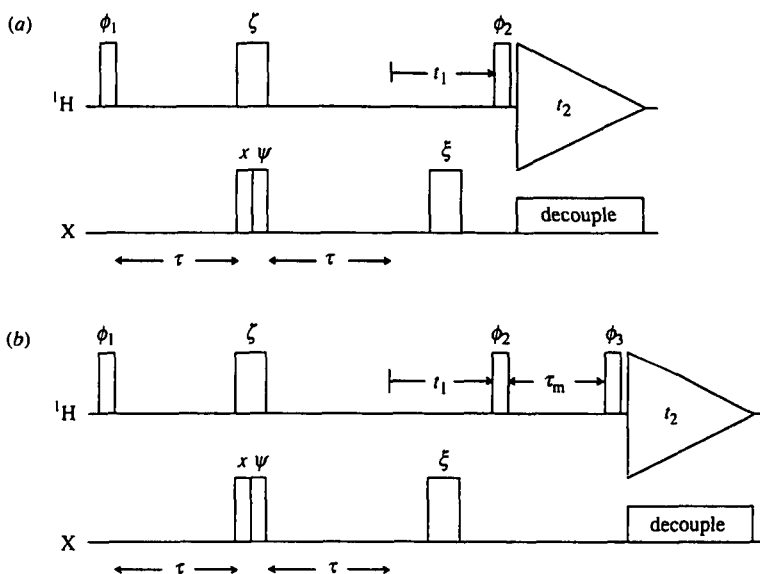
Fig. 22. Experimental schemes with $X(\omega_1)$-half-filter and heteronuclear broadband decoupling. (a) [^{1}H,^{1}H]-COSY. (b) [^{1}H,^{1}H]-NOESY. The phase cycles are described in the text.

$$
\begin{aligned}
&\text{[}^1\text{H,}^1\text{H]-NOESY with } X(\omega_1)\text{-half-filter and refocusing}\\
&\text{H}_z \xrightarrow{\hspace{5cm}} \pm \cos \Omega t_1\, \text{H}_x\\
&\text{I}_z \xrightarrow{\hspace{5cm}} -\cos \Omega t_1\, \text{I}_x.
\end{aligned}
\right\} \tag{18}
$$

Comparison with equations (13) and (14) shows that the same result is obtained as in an experiment with $X(\omega_2)$-half-filter and refocusing, except for trivial differences in the signs and the phases. (Remember that the equations used here describe the diagonal peaks. For cross-peaks the roles of the ω_1 and ω_2 frequency axes are interconverted between experiments with $X(\omega_1)$-half-filter, or $X(\omega_2)$-half-filter, respectively.) The experimental scheme of Fig. 22b was applied, for example, to ^{15}N-labelled T$_4$-phage lysozyme (McIntosh et al. 1987), and to the N-terminal DNA-binding domain of λ-repressor, which had been enriched to 60% in the C$^\beta$-position of the alanines (Bax & Weiss, 1987).

6. 2D [^{1}H,^{1}H]-NMR WITH nX-DOUBLE-HALF-FILTERS

A nX-double-half-filter is obtained with the use of a $nX(\omega_1)$-half-filter and a $nX(\omega_2)$-half-filter in the same 2D [^{1}H,^{1}H]-NMR experiment (Otting & Wüthrich, 1989). In the resulting experimental scheme the two half-filter elements function independently of each other. For example, they can be applied to different heteronuclei, e.g. ^{13}C and ^{15}N, and they can be tuned to different heteronuclear coupling constants. Combined with suitable isotope labelling, this opens almost unlimited possibilities for extensive editing of complex 2D [^{1}H,^{1}H]-NMR spectra. So far only very few of these possible filter combinations have been used in practice, and higher-order double-half-filters with $n > 1$ have not yet been implemented. The following discussion will therefore focus on $X(\omega_1,\omega_2)$-double-half-filters with a single heteronuclear species X and with $n = 1$.

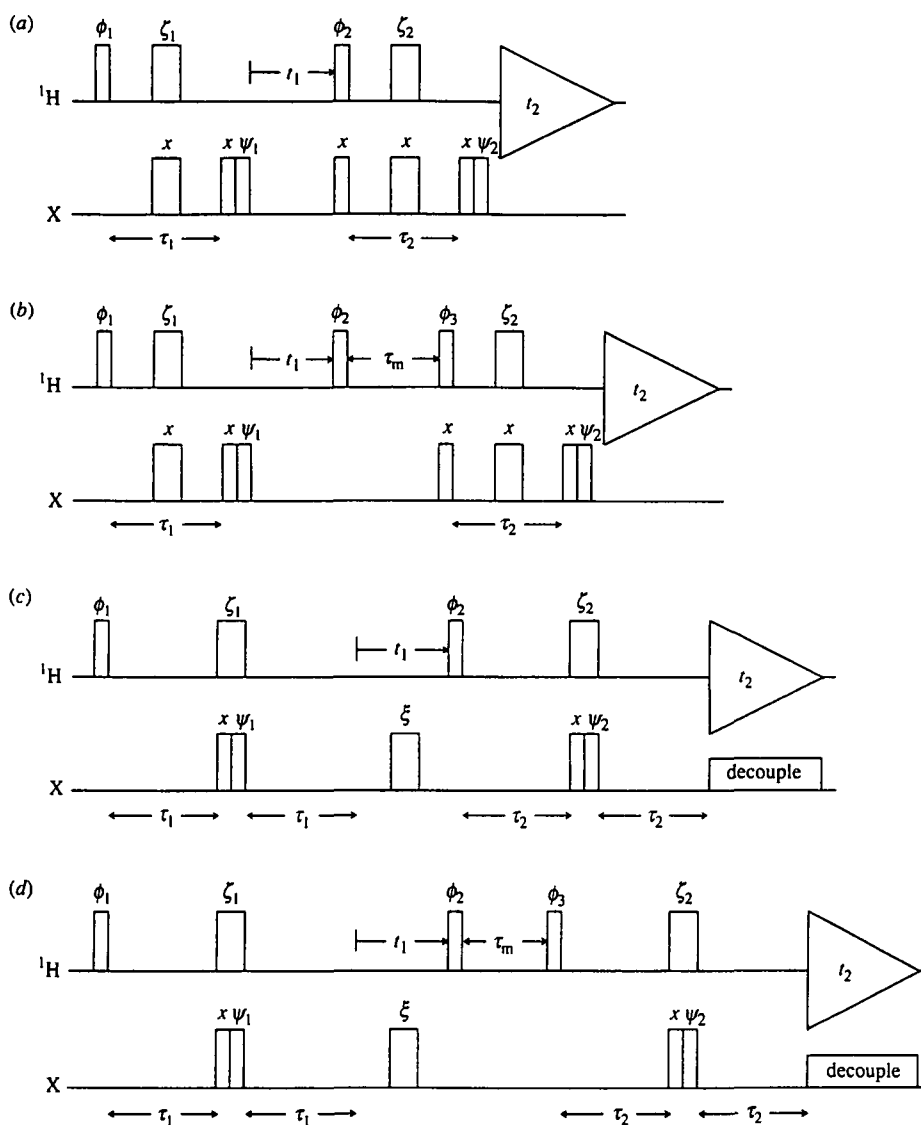Fig. 23. Experimental schemes with heteronuclear double-half-filters. (*a*) [¹H,¹H]-COSY with X(ω_1,ω_2)-double-half-filter. (*b*) [¹H,¹H]-NOESY with X(ω_1,ω_2)-double-half-filter. (*c*) [¹H,¹H]-COSY with X(ω_1,ω_2)-double-half-filter and heteronuclear decoupling. (*d*) [¹H,¹H]-NOESY with X(ω_1,ω_2)-double-half-filter and heteronuclear decoupling.

6.1 *[¹H,¹H]-COSY and [¹H,¹H]-NOESY with X(ω_1, ω_2)-double-half-filter*

Fig. 23 shows experimental schemes of [¹H,¹H]-COSY and [¹H,¹H]-NOESY with X-double-half-filters. The phases ψ_1 and ψ_2 of the editing pulses in each of the two X-half-filter elements are cycled independently between x and $-x$. The resulting four possible combinations, I–IV (Table 4) are stored separately. Suitable linear combinations of the data sets I–IV yield four different subspectra (Table 5). First, the sum of all four data files contains all those signals that are not

Table 4. *Phase cycling of ψ_1 and ψ_2 used for the four recordings in the $X(\omega_1,\omega_2)$-double-half-filter experiments of Fig. 23*

Recording	ψ_1	ψ_2
I	x	x
II	$-x$	x
III	x	$-x$
IV	$-x$	$-x$

Table 5. *Desired subspectra obtained as linear combinations of the four data sets defined in Table 4, which were recorded with a $^{13}C(\omega_1,\omega_2)$-double-half-filter*

| Subspectrum	Combination of recordings	Filter pass characteristics
$^{13}C(\omega_1)$–$^{13}C(\omega_2)$-doubly-filtered	I+II+III+IV	Unlabelled resonances in ω_1 and ω_2
$^{13}C(\omega_1)$-filtered/ $^{13}C(\omega_2)$-selected	(I+II)–(III+IV)	^{13}C labelled in ω_2, unlabelled in ω_1
$^{13}C(\omega_1)$-selected/ $^{13}C(\omega_2)$-filtered	(I–II)+(III–IV)	^{13}C labelled in ω_1, unlabelled in ω_2
$^{13}C(\omega_1)$–$^{13}C(\omega_2)$-doubly-selected	(I–II)–(III–IV)	^{13}C labelled in ω_1 and ω_2

affected by either of the two editing pulses, and therefore this subspectrum includes the diagonal peaks and cross-peaks from the protons that are not bound to X. The expression 'X(ω_1)–X(ω_2)-doubly-filtered' was chosen for the sum spectrum, since for exactly matched half-filter delays $\tau_1 = 1/2\,^1\!J(^1H,X)$ and $\tau_2 = 1/2\,^1\!J(^1H',X')$ the peaks involving resonances from X-bound protons are suppressed in this subspectrum (Table 3). The second combination of the data sets I–IV in Table 5 selects those magnetizations which are insensitive to the phase ψ_1 of the X(ω_1)-half-filter, but change their sign with the phase ψ_2 of the X(ω_2)-half-filter. They correspond to the signals usually observed in an experiment with X(ω_2)-half-filter, except that along ω_1 there are only resonances from protons not bound to X. This additional X(ω_1) filtering effect results in efficient suppression of all diagonal peaks, since each diagonal peak arises either entirely from a labelled proton, or entirely from an unlabelled proton. The third linear combination of Table 5 leads to the same result as the second one, except that the roles of ω_1 and ω_2 are interchanged. The fourth combination of Table 5 leads to a subspectrum which contains exclusively signals originating from X-bound protons, including the diagonal peaks of the X-bound protons. The sum of all four subspectra listed in Table 5 would give the complete spectrum, as it would be observed without the X-double-half-filter. As in the experiments with X-half-filters, there is no loss in sensitivity when a X-double-half-filter is inserted into a 2D [^1H,^1H]-NMR experiment, always provided that the influence of pulse imperfections and the

relaxation during the filter delays can be neglected. It is a new feature, which is not available with X-half-filters, that X-double-half-filters can separate cross peaks between X-bound protons and unlabelled protons from the correlations between different X-bound protons.

An experimental scheme with $X(\omega_1,\omega_2)$-double-half-filter can be constructed with either of the X-half-filter elements of Fig. 14 (*a* or *c*), depending on whether heteronuclear broadband decoupling is desired or not. Fig. 23 (*a*, *b*), shows the experimental schemes for [¹H,¹H]-COSY and [¹H,¹H]-NOESY with X-double-half-filter without refocusing. The presence of the $X(\omega_2)$-half-filter calls for a $(\pi/2)(X)$-pulse during the mixing period, to prevent cross talk from the difference spectrum into the sum spectrum (see section 5.2.1). Complete multiplets rather than the E. COSY-type multiplet patterns will then be observed (see section 5.2.5). If it is desirable to simplify the spectrum by heteronuclear decoupling along both frequency axes, this can be achieved with the experimental schemes of Fig. 23 (*c*, *d*). For all the experimental schemes of Fig. 23 the phase cycle includes the basic steps of the [¹H,¹H]-COSY or [¹H,¹H]-NOESY experiment, respectively, and is extended by independent cycling of the phases ζ_1 and ζ_2 of the π(¹H)-pulses [Fig. 23 (*a–d*)] and of the phase ξ of the refocusing π(X)-pulse [Fig. 23 (*c*, *d*)]. The receiver phase is the same as in the conventional [¹H,¹H]-COSY and [¹H,¹H]-NOESY experiments (Figs 10, 11) and is not changed together with the phase alternations of the π-pulses (Fig. 14 *d*). The phase-cycling priority list for [¹H,¹H]-NOESY with $X(\omega_1,\omega_2)$-double-half-filter and decoupling (Fig. 23 *d*) is: ψ_1, ψ_2, 2-step CYCLOPS, ϕ_3, ϕ_2, ζ_1, ζ_2, ξ, ϕ_1 and repetition with permuted order of ψ_1 and ψ_2. The resulting phase cycle would consist of 2048 steps. It can be shortened to 256 steps without significant loss in performance by omission of the permuted repetition (see sections 3.3.3 and 7) and by replacing the refocusing π(X) pulse of phase ξ with broadband decoupling. Phase programs for the other experimental schemes of Fig. 23 can be derived from the same phase-cycle priority list.

6.2 *Experimental examples*

The NOESY pulse scheme of Fig. 23 *d* was used to record the four sub-spectra of Table 5 with a preparation of P22 c2 repressor 1–76 in which one of the methyl groups of each of the four valyl residues (Fig. 6) was enriched with ¹³C to about 40 %, whereby this labelling was not stereo-specific (Fig. 24). The spectral region shown contains the diagonal peaks of all eight valyl methyl groups. Fig. 24 *a* shows the $^{13}C(\omega_1)$–$^{13}C(\omega_2)$-doubly-filtered sum spectrum, which contains in both dimensions the resonances from ^{12}C-bound protons. Fig. 24 (*b*, *c*), show the $^{13}C(\omega_1)$-filtered/$^{13}C(\omega_2)$-selected subspectrum, and the $^{13}C(\omega_1)$-selected/$^{13}C(\omega_2)$-filtered subspectrum, respectively. The diagonal peak suppression is readily apparent in these two subspectra. The diagonal peaks of the ^{13}C-bound protons are found only in the $^{13}C(\omega_1)$–$^{13}C(\omega_2)$-doubly-selected subspectrum (Fig. 24 *d*). The two cross-peaks seen in this spectrum are between the ^{13}C-enriched methyl groups of two different Val residues. Clearly, the improved resolution in the subspectra (*b*)–(*d*) of Fig. 24 greatly facilitates the spectral analysis. Although the
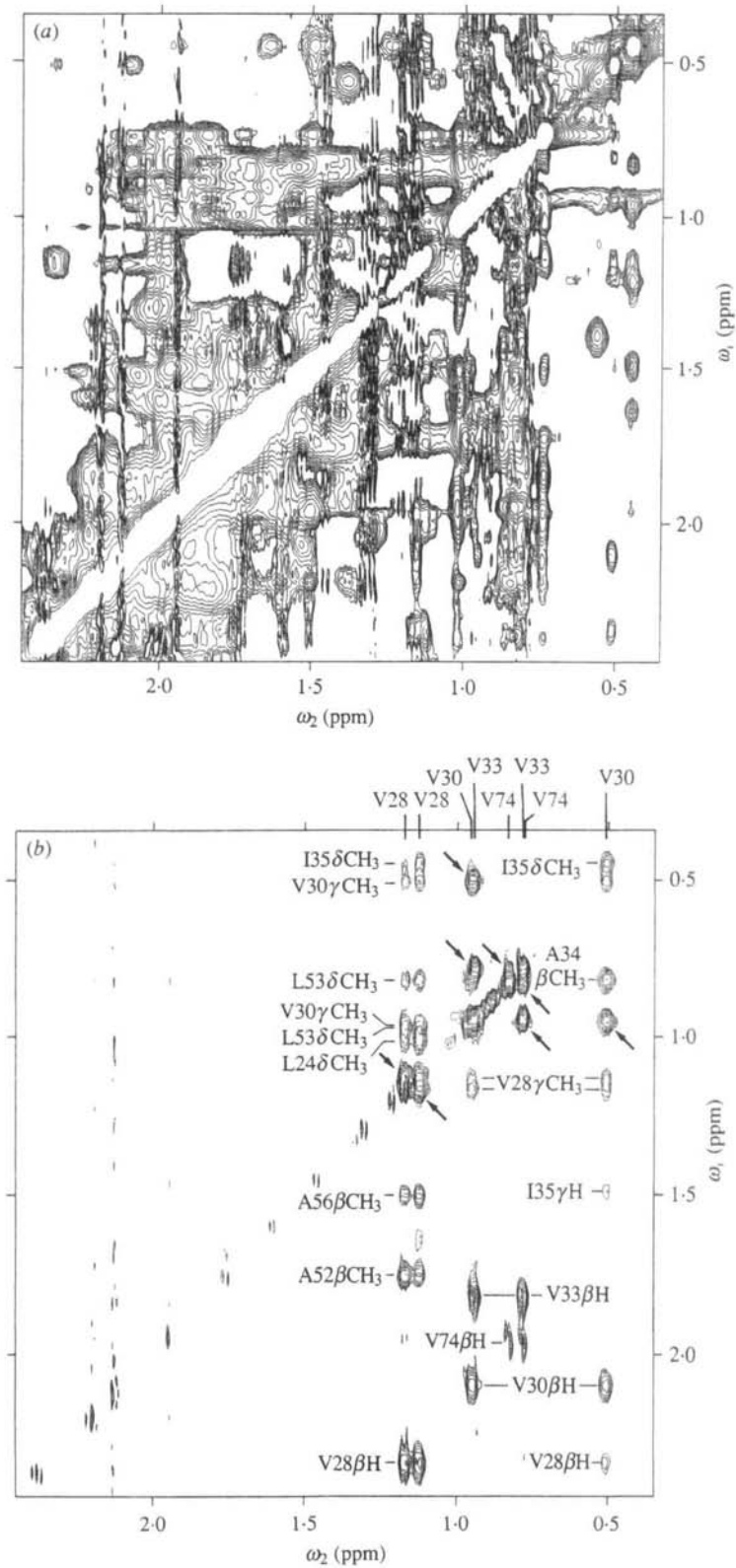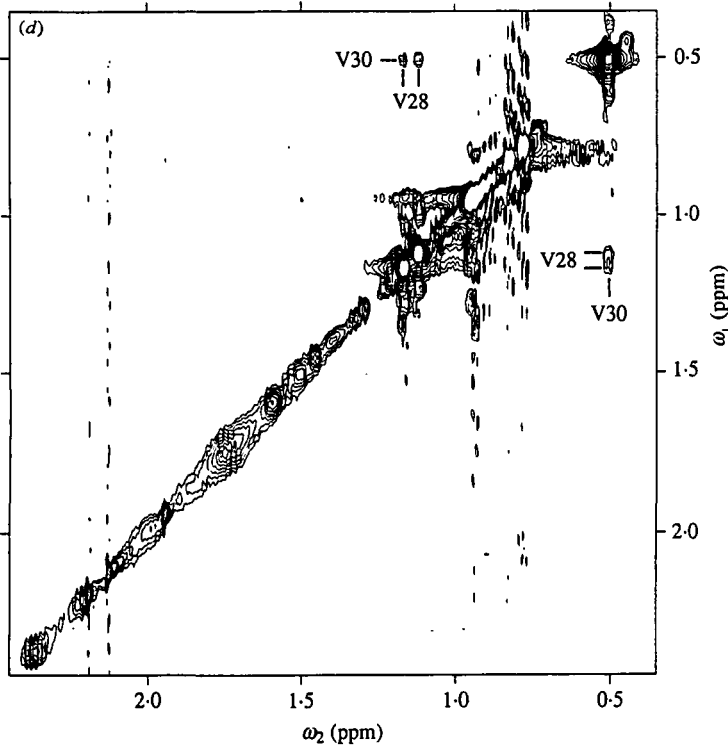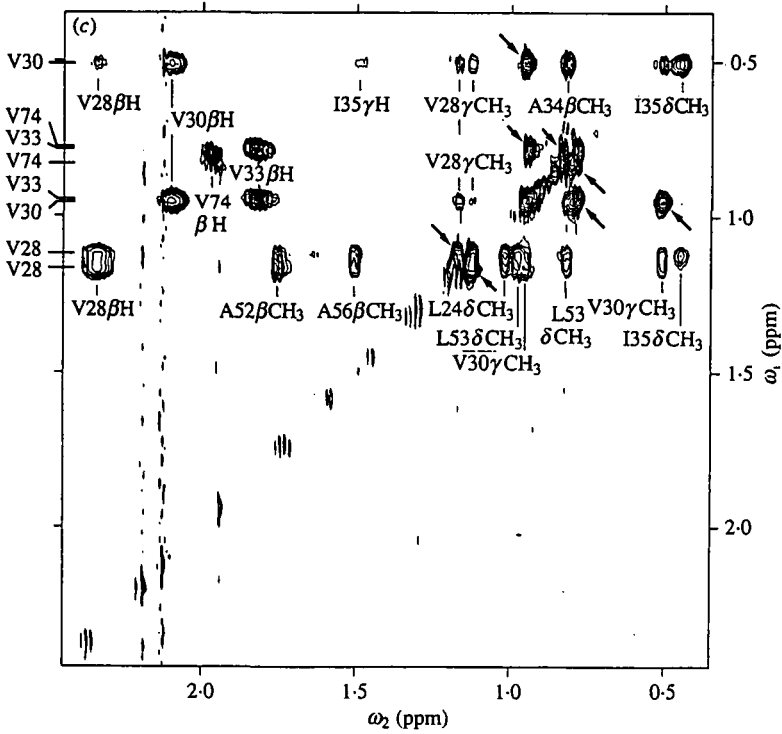
Fig. 24. For legend see p. 88.

subspectra of Fig. 24 (*b*, *c*), contain basically the same information (Table 1), the fine structure of the cross peaks is better resolved along ω_2 then along ω_1 because of the higher digital resolution along ω_2. The subspectra (*b*) and (*c*) are therefore complementary with respect to this information content about the multiplet fine structures and the precise resonance frequencies of the protons involved in the cross-peaks. A further advantage of the use of the $X(\omega_1,\omega_2)$-double-half-filter lies in the fact that the t_1 noise associated with intense diagonal peaks is largely suppressed in the $X(\omega_1)$-filtered/$X(\omega_2)$-selected subspectrum and the $X(\omega_1)$-selected/$X(\omega_2)$-filtered subspectrum [Fig. 24 (*b*, *c*)].

The $X(\omega_1,\omega_2)$-double-half-filter offers an elegant way to separate cross-peaks between two X-bound protons from those between X-labelled and unlabelled proton resonances. A particularly attractive application is for studies of fractionally ^{13}C-labelled compounds. Here, this is illustrated with the stereospecific assignments of the diastereotopic methyl groups of Val and Leu in the DNA-binding domain 1–69 of the 434-phage repressor. The protein preparation used for this experiment was isolated from an overexpression system in *E. coli* grown on a minimal medium containing glucose as the only carbon source. About 10 % of the glucose was uniformly enriched with ^{13}C in the extent of 99 %, and 90 % of the glucose contained the natural isotope distribution with 1.1 % ^{13}C. On average, each carbon position in the protein thus obtained contained about 10 % ^{13}C. With a purely statistical isotope distribution, the probability of finding molecular fragments with two neighbouring ^{13}C atoms would be 1 %, if the contributions from the natural abundance of ^{13}C are neglected. However, the biosynthetic pathways in the bacteria ensure that certain C–C fragments are doubly labelled. In the isopropyl groups of Val and Leu this biosynthetically directed fractional ^{13}C labelling (Senn *et al.* 1989; Neri *et al.* 1989) is stereoselective (Hill *et al.*, 1979; see also references in Neri *et al.* 1989). The pro-R-methyl carbon comes from the same glucose molecule as the adjoining methine carbon, so that the fragments CH–CH$_3$(pro-R) are doubly labelled with ^{13}C in the extent of the overall fractional labelling, i.e. in the present experiment 10 %. In contrast, the pro-S methyl carbon and the methine carbon come from

---

Fig. 24. [^{1}H,^{1}H]-NOESY with $^{13}C(\omega_1,\omega_2)$-double-half-filter of P22 c2 repressor 1–76. The protein was labelled in the extent of about 40 % with non-stereospecifically enriched [4-^{13}C]-Val. (Protein concentration 5 mM in D$_2$O, pD 4.8, 28 °C, τ_m = 100 ms, $\tau_1 = \tau_2 = 4.0$ ms, proton frequency 500 MHz, the experiment of fig. 23 *d* was used.) The spectral region (ω_1 = 0.4–2.4 ppm, ω_2 = 0.4–2.4 ppm) is shown, which contains the diagonal peaks of the eight Val methyl groups. All four subspectra (Tables 1 and 5) were processed and plotted with identical parameters. (*a*) $^{13}C(\omega_1)$–$^{13}C(\omega_2)$-doubly-filtered subspectrum. (*b*) $^{13}C(\omega_1)$-filtered/$^{13}C(\omega_2)$-selected subspectrum. (*c*) $^{13}C(\omega_1)$-selected/$^{13}C(\omega_2)$-filtered subspectrum. (*d*) $^{13}C(\omega_1)$–$^{13}C(\omega_2)$-doubly-selected subspectrum. At the top and on the left of the subspectra (*b*) and (*c*), respectively, the eight valyl methyl chemical shifts are identified with the one-letter amino-acid symbol and the sequence number. Intraresidual cross-peaks between the two methyl groups of the same valine side chain are identified arrows, and the interresidual cross-peaks with unlabelled protons are identified with the assignments of the latter. In (*d*) the cross-peaks between different ^{13}C-bound protons are identified with the sequence positions of the two interacting valines. (From Otting & Wüthrich, 1989.)

different source molecules, so that with an overall enrichment of 10% only approximately 1% of the CH–CH$_3$(pro-S) fragments are doubly labelled with ^{13}C. On this basis stereospecific assignments for the methyl NMR lines of Val and Leu in the native form of the protein can be obtained (Senn *et al.* 1989; Neri *et al.* 1989). Fig. 25 illustrates the use of [^{1}H,^{1}H]-COSY with a ^{13}C(ω_1,ω_2)-double-half-filter for distinguishing between ^{13}CH–^{13}CH fragments and ^{12}CH–^{13}CH fragments. The spectral region shown contains the resonance frequencies of the C$^\beta$-protons of Val and the C$^\gamma$-protons of Leu along ω_1, and the resonance frequencies of the methyl protons of these amino acids along ω_2. Fig. 25*a* shows the ^{13}C(ω_1)–^{13}C(ω_2)-doubly-filtered sum spectrum. This subspectrum contains the cross peaks between ^{12}C-bound protons. Since the protein is labelled only in the extent of 10%, the sum spectrum has the same appearance as a conventional [^{1}H,^{1}H]-COSY spectrum of the unlabelled protein. Fig. 25*b* shows the ^{13}C(ω_1)-filtered/^{13}C(ω_2)-selected subspectrum. The ^{13}C-filtering effect along ω_1 affords the selective observation of the cross-peaks between the unlabelled methine protons and the ^{13}C-labelled pro-S methyl protons in this subspectrum. The ^{13}C(ω_1)-selected/^{13}C(ω_2)-filtered subspectrum (not shown) contains the cross-peaks between ^{13}C-labelled methine protons and unlabelled methyl protons, and thus selects also the cross-peaks with the pro-S methyl groups. The absence of cross-peaks with the pro-R methyl group in Fig. 25*b* shows in a direct way that the two-carbon fragment consisting of the pro-R methyl group and the methine carbon comes from the same glucose molecule, so that it is either doubly labelled or doubly unlabelled. Fig. 25*c* shows the ^{13}C(ω_1)–^{13}C(ω_2)-doubly-selected subspectrum, which selects the cross-peaks between ^{13}C-labelled methine protons and ^{13}C-labelled protons of the pro-R methyl groups. For some of the Val and Leu residues weak cross-peaks with the protons of the pro-S methyl group are also seen. These arise from statistical double-labelling with ^{13}C atoms originating from different glucose molecules. Compared to alternative NMR experiments, e.g. [^{13}C,^{1}H]-COSY, which can also be used for obtaining these stereospecific assignments from the same protein preparation (Neri *et al.* 1989), the use of [^{1}H,^{1}H]-COSY with ^{13}C(ω_1,ω_2)-double-half-filter has the advantage that the stereospecific ^{1}H-NMR assignments can be obtained without the need to assign the ^{13}C-spectrum.

7. CROSS-TALK AS A LIMITING FACTOR IN THE USE OF HETERONUCLEAR HALF-FILTERS

In experiments with X-half-filters a principal source of cross talk between the different subspectra is the need to tune the delay τ of the X-half-filter elements to the heteronuclear coupling constants. First, as we have seen in metallothionein, the heteronuclear coupling constants in certain systems may vary over an order of magnitude, and the filter delay will necessarily represent a compromise between the optimum τ values for small and large coupling constants. Second, in work with macromolecules significant loss of magnetization can result from relaxation during the filter delays, so that the use of shorter filter delays may be indicated. The following product operator calculation describes the effects to be expected from
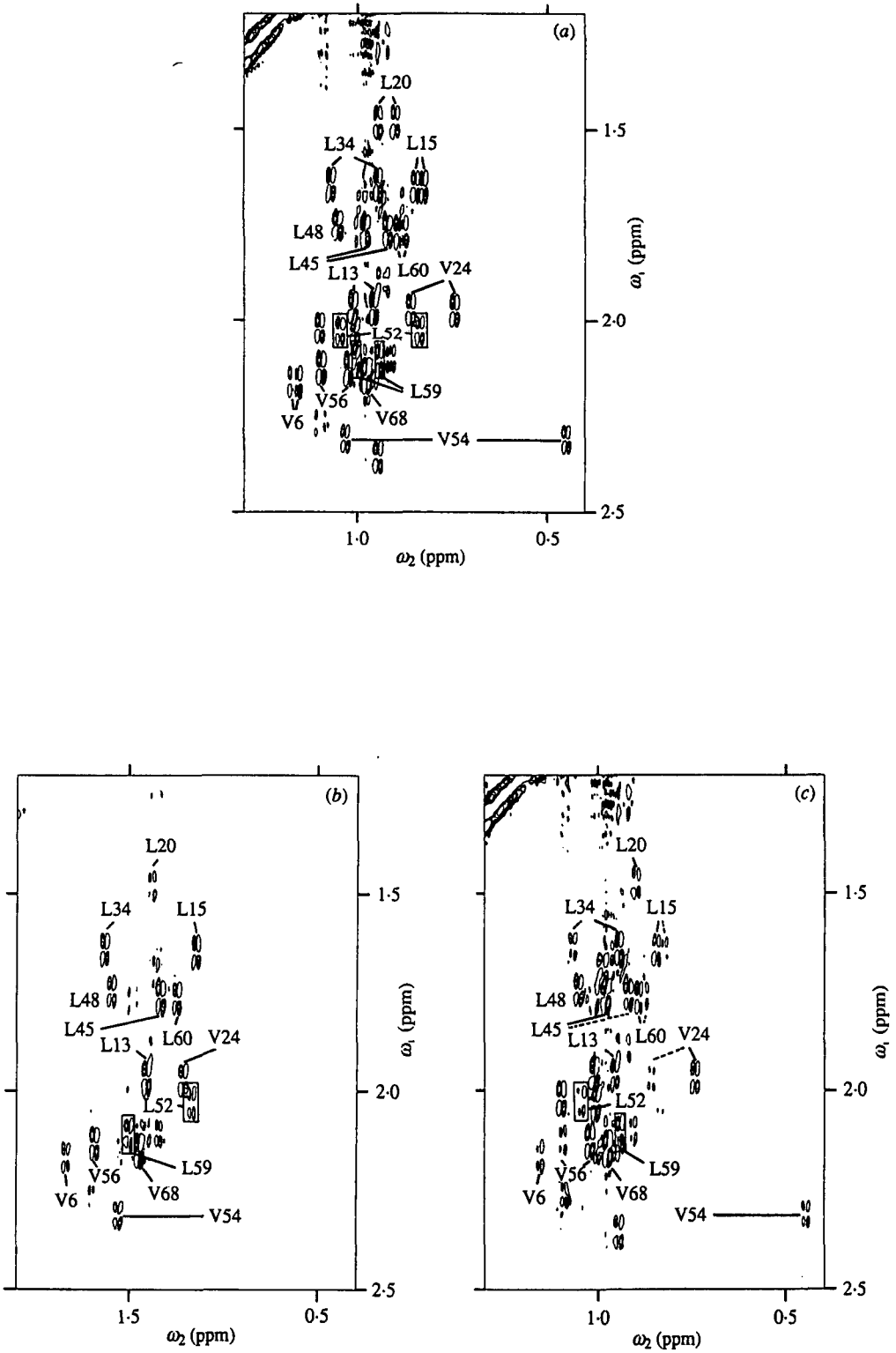
Fig. 25. For legend see opposite page.

deviations of the filter delay τ from the optimal tuning value of $\tau = 1/2\mathcal{J}_{HX}$. Starting from transverse magnetization H_x we have for the filter element of Fig. 14*a*

$$H_x \xrightarrow{\;\;\tau/2 - \pi_\zeta(^{1}H) - \pi_x(X) - \tau/2\;\;} \cos \pi\mathcal{J}_{HX}\,\tau\,H_x + \sin \pi\mathcal{J}_{HX}\,\tau\,2H_y\,X_z. \tag{19}$$

The following pair of $(\pi/2)(X)$-pulses, which includes the editing pulse (Fig. 14*a*), does not affect in-phase magnetization, irrespective of whether it is from a X-bound proton or from an unlabelled resonance. Therefore some signal intensity from X-bound protons will appear in the sum spectrum, if the delay τ deviates from the value $\tau = 1/2^{1}\mathcal{J}(^{1}H,X)$. The difference spectrum, however, always selects only the heteronuclear antiphase magnetization and is free of cross-talk from the sum spectrum. For the same reason no cross-talk is found in $X(\omega_1)$–$X(\omega_2)$-doubly-selected subspectra from experiments with X-double-half-filter. However, the $X(\omega_1)$–$X(\omega_2)$-doubly-selected subspectrum may leak into the $X(\omega_1)$-selected/$X(\omega_2)$-filtered subspectrum and into the $X(\omega_1)$-filtered/$X(\omega_2)$-selected subspectrum, and these three subspectra may all cross-talk into the $X(\omega_1)$–$X(\omega_2)$-doubly-filtered sum spectrum. These considerations on the filter element of Fig. 14*a* apply also to the X-half-filter element with refocusing (Fig. 14*c*). A mistuned delay τ again causes cross-talk from the difference spectrum into the sum spectrum. In addition, incomplete refocusing of the heteronuclear antiphase magnetization may cause phase distortions in the difference spectrum, unless the antiphase magnetization is destroyed by a heteronuclear broadband decoupling sequence.

A different source of cross-talk, which may be operative even with exact tuning to $\tau = 1/2\mathcal{J}_{HX}$, arises when the effective editing $\pi(X)$-pulse fails to completely invert the X_z-operators due to off-resonance effects or deviations from the nominal 180° flip angle. While the appearance of the difference spectrum would again be unaffected by such pulse imperfections, some of its intensity would leak into the sum spectrum.

If the data corresponding to different phase settings of the editing pulse are acquired in a scan-interleaved mode, spectrometer instabilities as a source of

---

Fig. 25. [^{1}H,^{1}H]-COSY spectrum of 434 repressor 1–69 recorded with a ^{13}C(ω_1,ω_2)-double-half filter and refocusing. The protein was enriched with ^{13}C in the extent of about 10 % by biosynthetically directed fractional ^{13}C-labelling. (Protein concentration 2 mM in D$_2$O, 25 mM phosphate buffer, 100 mM-KCl, pD = 6·0, 30 °C, filter delays: $\tau_1 = \tau_2 = 3\cdot6$ ms, $t_{1\,max} = 51$ ms, ^{1}H-frequency 600 MHz. The experiment of Fig. 23c was used.) The spectral region ($\omega_1 = 1\cdot2$–$2\cdot5$, $\omega_2 = 0\cdot4$–$1\cdot3$ ppm) is shown. Positive and negative peaks are distinguished by the fact that only the lowest contour line has been drawn for the positive peaks. The C$^\beta$H–C$^\gamma$H$_3$ cross-peaks of Val and the C$^\gamma$H–C$^\delta$H$_3$ cross-peaks of Leu are identified with the one-letter amino-acid symbol and the sequence number. Additional, unidentified peaks are from the Ile residues. For improved clarity, cross-peaks in crowded spectral areas are framed. (*a*) ^{13}C(ω_1)–^{13}C(ω_2)-doubly-filtered. This subspectrum contains the two methyl resonances of each isopropyl group of Val and Leu with equal intensity. Stereospecific assignments are not indicated. (*b*) ^{13}C(ω_1)-filtered/^{13}C(ω_2)-selected. The cross peaks with the pro-S methyl groups of Val and Leu are identified. (*c*) ^{13}C(ω_1)–^{13}C(ω_2)-doubly-selected. Solid and dashed lines identify the cross peaks with the pro-R and pro-S methyl groups, respectively.
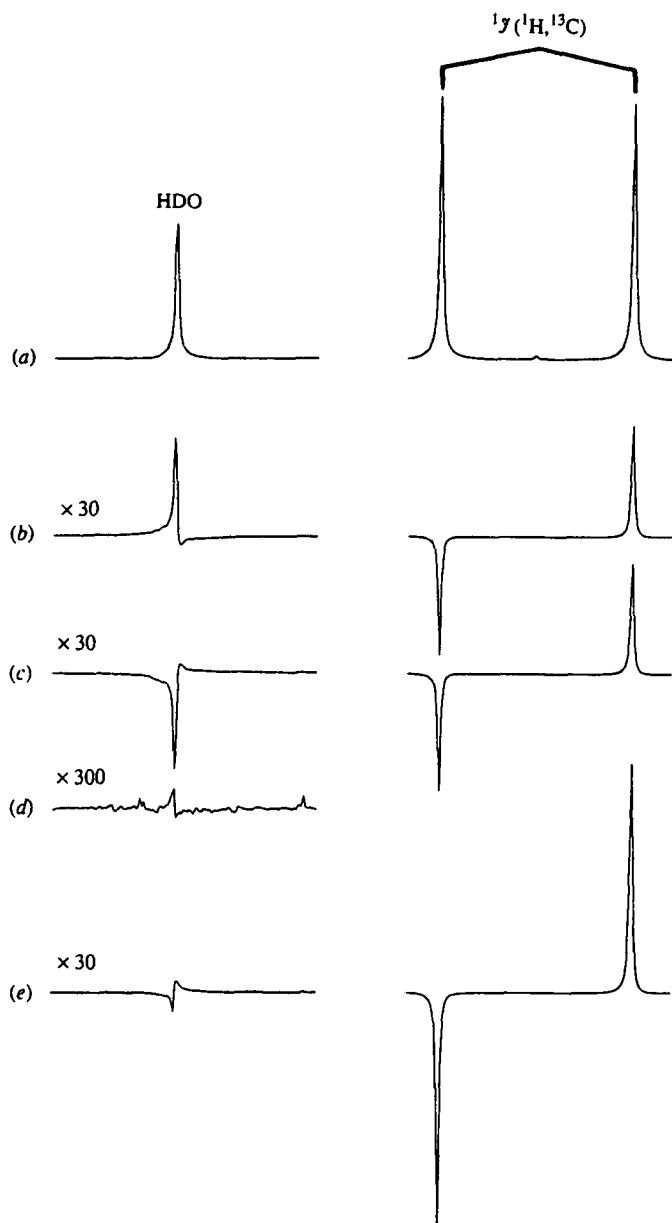
Fig. 26. Demonstration of cross-talk. (*a*) 1D ^{1}H-NMR spectrum of [2-^{13}C]-acetate in D_2O. 128 scans were accumulated. (*b*) Spectrum recorded with the same sample as in (*a*) using [^{1}H,^{1}H]-NOESY with ^{13}C(ω_2)-half-filter (Fig. 15*b*). 64 scans were accumulated, with the phase cycle priority list: ψ, 2-step CYCLOPS, Φ_3, Φ_2, ζ, Φ_1. In the phase cycle each scan with $\psi = x$ was *preceded* by the corresponding scan with $\psi = -x$. The data recorded with different phases ψ were subtractively combined to yield the difference spectrum shown. The residual HDO signal is plotted on a 30 times increased scale. (*c*) Same as (*b*), but each scan with $\psi = x$ was *followed* by the corresponding scan with $\psi = -x$. The residual HDO signal is plotted on a 30 times increased scale. (*d*) Residual HDO signal after addition of the spectra (*b*) and (*c*) plotted on a 300 times increased scale. (*e*) Same as (*b*), but 128 scans were recorded with the phase cycle priority list: 2-step CYCLOPS, Φ_3, Φ_2, ζ, Φ_1, ψ. In addition, four dummy scans were applied before each phase alternation of ψ. The residual HDO signal is plotted on a 30 times increased scale.

imperfect subtraction upon combination of the different data sets can largely be excluded. (In a scan-interleaved mode each scan for one data set is followed by the corresponding scan for the other data set.) If the relaxation delay between successive scans is too short to allow for complete relaxation, scan-interleaved acquisition may lead to a systematic bias of the signal amplitude between the two data sets recorded with $\psi = x$ and $\psi = -x$. (In work with macromolecules it is quite common to shorten the relaxation delay in order to improve the effective sensitivity.) The situation can be remedied by recording the two data sets in reversed order and coadding the corresponding data (Wörgötter *et al.* 1988). Fig. 26(*b–d*), demonstrates the results obtainable with this procedure. As a reference, Fig. 26*a* shows the conventional 1D spectrum of [2–^{13}C]-acetate in D$_2$O. The spectrum of Fig. 26*b* was recorded with the [^{1}H,^{1}H]-NOESY scheme with ^{13}C(ω_2)-half-filter (Fig. 15*b*), using the first half of the 128-step phase cycle of section 5.2.1 with the phase cycling priority list: ψ, 2-step CYCLOPS, ϕ_3, ϕ_2, ζ, and ϕ_1. Fig. 26*c* shows the spectrum obtained using the second half of the 128-step phase cycle, with permuted order of ψ. In both experiments the evolution period t_1 was set to 3 μs so that the data correspond to the first t_1 increment of the 2D experiment. The difference spectra are shown, which result from subtraction of the two free induction decays belonging to the different phases of the $(\pi/2)_\psi$(X) editing pulse. The doublet from the ^{13}CH$_3$ protons is antiphase with respect to the heteronuclear coupling, the HDO signal is reduced approximately by a factor 15 relative to its intensity in the reference spectrum of Fig. 26*a* and the sign of the residual HDO line in (*c*) is reversed relative to (*b*). The sum of the spectra of Fig. 26(*b, c*), leads to the residual HDO signal shown in Fig. 26*d*, which is reduced by more than a factor 1000 relative to the reference spectrum of Fig. 26*a*. This excellent suppression can only be obtained with the complete phase cycle, which includes the repetition with permuted order of ψ. For situations where the ensuing long overall measuring time is not acceptable, a shorter phase-cycling scheme may be used, which does not include the repetition with permuted order of ψ and still reduces the residual HDO signal by more than a factor 100 compared to the reference spectrum (Fig. 26*e*). In this experiment the same phase cycle is used as in the spectrum of Fig. 26*b*, except that the phase ψ was cycled as the last step rather than the first step. In addition, several dummy scans were inserted before the switching of the phase ψ to avoid the build-up of a systematic bias between the two data sets, which might result from insufficient relaxation between the scans with different ψ. [Although this phase cycle contains only 64 steps, 128 scans were accumulated to allow a direct comparison with Fig. 26(*a, d*).]

From the comparison of the spectra (*d*) and (*e*) in Fig. 26 it is clear that the full phase cycle including the repetition with permuted order of ψ (Wörgötter *et al.* 1988) should be used whenever this can be afforded in terms of the overall measurement time available. The permutation of the phase cycle has also been found to improve the quality of proton-detected [^{13}C,^{1}H]-COSY spectra with natural abundance samples (Cavanagh & Keeler, 1988). When assessing the practical significance of the observations made in Fig. 26, one should also keep in mind that the results depend critically on the relaxation delay between successive scans (in all the experiments of Fig. 26 the repetition rate was 1·8 s per scan). For

example, as one would expect for artefacts which come from insufficient relaxation between successive scans, the amplitude of the residual HDO signal in Fig. 26, *b* and *c*, is significantly reduced when longer relaxation delays are employed.

8. ACKNOWLEDGEMENTS

9. REFERENCES

ARSENIEV, A., SCHULTZE, P., WÖRGÖTTER, E., BRAUN, W., WAGNER, G., VAŠÁK, M., KÄGI, J. H. R. & WÜTHRICH, K. (1988). Three-dimensional structure of rabbit liver [Cd₇]-metallothionein-2a in aqueous solution determined by nuclear magnetic resonance. *J. molec. Biol.* **201**, 637–657.

AUE, W. P., BARTHOLDI, E. & ERNST, R. R. (1976). Two-dimensional spectroscopy. Application to nuclear magnetic resonance. *J. Chem. Phys.* **64**, 2229–2246.

BAX, A. & DAVIS, D. G. (1985). MLEV-17-based two-dimensional homonuclear magnetization transfer spectroscopy. *J. magn. Reson.* **65**, 355–360.

BAX, A. & WEISS, M. A. (1987). Simplification of two-dimensional NOE spectra of proteins by ^{13}C labeling. *J. magn. Reson.* **71**, 571–575.

BAX, A., GRIFFEY, R. H. & HAWKINS, B. L. (1983). Correlation of proton and nitrogen-15 chemical shifts by multiple quantum NMR. *J. magn. Reson.* **55**, 301–315.

BODENHAUSEN, G., FREEMAN, R. & TURNER, D. L. (1977). Suppression of artifacts in two dimensional J spectroscopy. *J. magn. Reson.* **27**, 511–514.

BODENHAUSEN, G., KOGLER, H. & ERNST, R. R. (1984). Selection of coherence-transfer pathways. *J. magn. Reson.* **58**, 370–388.

BOLTON, P. H. (1985). Heteronuclear relay transfer spectroscopy with proton detection. *J. magn. Reson.* **62**, 143–146.

BYSTROV, V. F. (1976). Spin–spin coupling and the conformational states of peptide systems. *Prog. NMR Spectrosc.* **10**, 41–81.

CAVANAGH, J. & KEELER, J. (1988). Improvement of carbon-13 satellite spectra by double difference spectroscopy. *J. magn. Reson.* **77**, 356–362.

EMSHWILLER, M., HAHN, E. L. & KAPLAN, D. (1960). Pulsed nuclear resonance spectroscopy. *Phys. Rev.* **118**, 414–424.

ERNST, R. R., BODENHAUSEN, G. & WOKAUN, A. (1987). *Principles of Nuclear Magnetic Resonance in One and Two dimensions.* Clarendon Press, Oxford.

FESIK, S. W. (1988). Isotope-edited NMR spectroscopy. *Nature* **332**, 865–866.

FESIK, S. W. & ZUIDERWEG, E. R. P. (1990). Heteronuclear three-dimensional NMR spectroscopy of isotopically labelled biological macromolecules. *Quart. Rev. Biophys.* (in press).

FESIK, S. W., GAMPE, JR., R. T. & ROCKWAY, T. W. (1987). Application of isotope-filtered 2D NOE experiments in the conformational analysis of atrial natriuretic factor(7–23). *J. magn. Reson.* **74**, 366–371.

FESIK, S. W., LULY, J. R., ERICKSON, J. W. & ABAD-ZAPATERO, C. (1988). Isotope-edited proton NMR study on the structure of a pepsin/inhibitor complex. *Biochemistry* **27**, 8297–8301.

FESIK, S. W., GAMPE, JR., R. T., ZUIDERWEG, E. R. P., KOHLBRENNER, W. E. & WEIGL, D. (1989). Heteronuclear three-dimensional NMR spectroscopy applied to CMP-KDO-synthetase (27·5 kDa). *Biochem. Biophys. Res. Commun.* **159**, 842–847.

FREEMAN, R., MARECI, T. H. & MORRIS, G. A. (1981). Weak satellite signals in high-resolution NMR spectra: separating the wheat from the chaff. *J. magn. Reson.* **42**, 341–345.

FREY, M. H., WAGNER, G., VAŠÁK, M., SØRENSEN, O. W., NEUHAUS, D., WÖRGÖTTER, E., KÄGI, J. H. R., ERNST, R. R. & WÜTHRICH, K. (1985). Polypeptide-metal cluster connectivities in metallothionein-2 by novel ¹H–¹¹³Cd heteronuclear two-dimensional NMR experiments. *J. Am. Chem. Soc.* **107**, 6847–6851.

GRIESINGER, C., SØRENSEN, O. W. & ERNST, R. R. (1986). Correlation of connected transitions by two-dimensional NMR spectroscopy. *J. Chem. Phys.* **85**, 6837–6852.

GRIESINGER, C., OTTING, G., WÜTHRICH, K. & ERNST, R. R. (1988). Clean TOCSY for ¹H spin system identification in macromolecules. *J. Am. Chem. Soc.* **110**, 7870–7872.

GRIFFEY, R. H. & REDFIELD, A. G. (1987). Proton-detected heteronuclear edited and correlated nuclear magnetic resonance and nuclear Overhauser effect in solution. *Quart. Rev. Biophys.* **19**, 51–82.

HILL, R. K., SAWADA, S. & ARFIN, S. M. (1979). Stereochemistry of valine and isoleucine biosynthesis. IV. Synthesis, configuration and enzymatic specificity of α-acetolactate and α-aceto-α-hydroxy-butyrate. *Bioorg. Chem.* **8**, 175–189.

HOULT, D. I. & RICHARDS, R. E. (1975). Critical factors in the design of sensitive high resolution nuclear magnetic resonance spectrometers. *Proc. R. Soc. Lond.* A**344**, 311–340.

KARPLUS, M. (1959). Contact electron-spin coupling of nuclear magnetic moments. *J. Chem. Phys.* **30**, 11–15.

MACURA, S., HUANG, Y., SUTER, D. & ERNST, R. R. (1981). Two-dimensional chemical exchange and cross-relaxation spectroscopy of coupled nuclear spins. *J. magn. Reson.* **43**, 259–281.

MARION, D., KAY, L. E., SPARKS, S. W., TORCHIA, D. A. & BAX, A. (1989). Three-dimensional heteronuclear NMR of ¹⁵N-labelled proteins. *J. Am. Chem. Soc.* **111**, 1515–1517.

MCINTOSH, L. P., DAHLQUIST, F. W. & REDFIELD, A. G. (1987). Proton NMR and NOE structural and dynamic studies of larger proteins and nucleic acids aided by isotope labels: T4 lysozyme. *J. Biomol. Struct. Dynamics* **5**, 21–34.

MESSERLE, B. A., WIDER, G., OTTING, G., WEBER, C. & WÜTHRICH, K. (1989). Solvent suppression using a spin lock in 2D and 3D NMR spectroscopy with H_2O solution. *J. magn. Reson.* **85**, 608–613.

MONTELIONE, G. T., WINKLER, M. E., RAUENBUEHLER, P. & WAGNER, G. (1989). Accurate measurements of long-range heteronuclear coupling constants from homonuclear 2D NMR spectra of isotope-enriched proteins. *J. magn. Reson.* **82**, 198–204.

NERI, D., SZYPERSKI, T., OTTING, G., SENN, H. & WÜTHRICH, K. (1989). Stereospecific nuclear magnetic resonance assignments of the methyl groups of valine and leucine in the DNA-binding domain of the 434 repressor by biosynthetic fractional ¹³C labelling. *Biochemistry* **28**, 7510–7516.

NEUHAUS, D., WAGNER, G., VAŠÁK, M., KÄGI, J. H. R. & WÜTHRICH, K. (1984). ¹¹³Cd–¹H spin–spin couplings in homonuclear ¹H correlated spectroscopy of metallothionein. Identification of the cysteine ¹H spin systems. *Eur. J. Biochem.* **143**, 659–667.

OTTING, G. & WÜTHRICH, K. (1988). Efficient purging scheme for proton-detected heteronuclear two-dimensional NMR. *J. magn. Reson.* **76**, 569–574.

OTTING, G. & WÜTHRICH, K. (1989). Extended heteronuclear editing of 2D ¹H NMR spectra of isotope-labelled proteins: the X(ω_1,ω_2)-double-half-filter. *J. magn. Reson.* **85**, 586–594.

OTTING, G., SENN, H., WAGNER, G. & WÜTHRICH, K. (1986). Editing of 2D ¹H NMR spectra using X-half-filters. Combined use with residue-selective ¹⁵N-labelling of proteins. *J. magn. Reson.* **70**, 500–505.

PIANTINI, U., SØRENSEN, O. W. & ERNST, R. R. (1982). Multiple-quantum filters for elucidating NMR coupling networks. *J. Am. Chem. Soc.* **104**, 6800–6801.

SCHULTZE, P., WÖRGÖTTER, E., BRAUN, W., WAGNER, G., VAŠÁK, M., KÄGI, J. H. R. & WÜTHRICH, K. (1988). Conformation of [Cd₇]-metallothionein-2 from rat liver in aqueous solution determined by nuclear magnetic resonance spectroscopy. *J. molec. Biol.* **203**, 251–268.

SENN, H., EUGSTER, A., OTTING, G., SUTER, F. & WÜTHRICH, K. (1987a). ¹⁵N-labeled P22 c2 repressor for nuclear magnetic resonance studies of protein-DNA interactions. *Eur. Biophys. J.* **14**, 301–306.

SENN, H., OTTING, G. & WÜTHRICH, K. (1987b). Protein structure and interactions by combined use of sequential NMR assignments and isotope labeling. *J. Am. Chem. Soc.* **109**, 1090–1092.

SENN, H., WERNER, B., MESSERLE, B. A., WEBER, C., TRABER, R. & WÜTHRICH, K. (1989). Stereospecific assignment of the methyl ¹H-NMR lines of valine and leucine in polypeptides by nonrandom ¹³C labelling. *FEBS Lett.* **249**, 113–118.

SØRENSEN, O. W., EICH, G. W., LEVITT, M. H., BODENHAUSEN, G. & ERNST, R. R. (1983). Product operator formalism for the description of NMR pulse experiments. *Prog. NMR Spectrosc.* **16**, 163–192.

SOUTH, T. L., KIM, B. & SUMMERS, M. F. (1989). ¹¹³Cd NMR studies of a 1:1 Cd adduct with an 18-residue finger peptide from HIV-1 nucleic acid binding protein, p7. *J. Am. Chem. Soc.* **111**, 395–396.

TORCHIA, D. A., SPARKS, S. W. & BAX, A. (1989). Staphylococcal nuclease: sequential assignments and solution structure. *Biochemistry* **28**, 5509–5524.

WILDE, J. A., BOLTON, P. H., STOLOWICH, N. J. & GERLT, J. A. (1986). A method for the observation of selected proton NMR resonances of proteins. *J. magn. Reson.* **68**, 168–171.

WÖRGÖTTER, E., WAGNER, G. & WÜTHRICH, K. (1986). Simplification of two-dimensional ¹H NMR spectra using an X-filter. *J. Am. Chem. Soc.* **108**, 6162–6167.

WÖRGÖTTER, E., WAGNER, G., VAŠÁK, M., KÄGI, J. H. R. & WÜTHRICH, K. (1988). Heteronuclear filters for two-dimensional ¹H-NMR. Identification of the metal-bound amino acids in metallothionein and observation of small heteronuclear long-range couplings. *J. Am. Chem. Soc.* **110**, 2388–2393.

WÜTHRICH, K. (1986). *NMR of Proteins and Nucleic Acids.* Wiley, New York.

WÜTHRICH, K. (1989). Protein structure determination in solution by nuclear magnetic resonance spectroscopy. *Science* **243**, 45–50.

WÜTHRICH, K., WIDER, G., WAGNER, G. & BRAUN, W. (1982). Sequential resonance assignments as a basis for determination of spatial protein structures by high resolution proton nuclear magnetic resonance. *J. molec. Biol.* **155**, 311–319.

WÜTHRICH, K., BILLETER, M. & BRAUN, W. (1984). Polypeptide secondary structure determination by nuclear magnetic resonance observation of short proton–proton distances. *J. molec. Biol.* **180**, 715–740.